

https://doi.org/10.1093/petrology/egac065
Original Manuscript

Trace and Rare Earth Element Compositions of Lawsonite as a Chemical Tracer of Metamorphic Processes in Subduction Zones

Patricia Kang^{1,*}, Donna L. Whitney¹, Laure A. J. Martin² and Katherine F. Fornash³

- ¹Department of Earth & Environmental Sciences, University of Minnesota, Minneapolis, MN 55455, USA
- ²Centre for Microscopy, Characterisation and Analysis, The University of Western Australia, Western Australia 6009, Australia
- ³Department of Geological Sciences, Ohio University, Athens, OH 45701, USA

Abstract

Lawsonite is a major host mineral of trace elements (TEs; e.g. REE, Sr, Pb, U, Th) and H2O in various rock types (metabasite, metasediment, metasomatite) over a wide range of depths in subduction zones. Consequently, the composition of lawsonite is a useful archive to track chemical exchanges that occurred during subduction and/or exhumation, as recorded in high-pressure/lowtemperature (HP/LT) terranes. This study provides an extensive dataset of major element and TE compositions of lawsonite in HP/LT rocks from two melanges (Franciscan/USA; Rio San Juan/Dominican Republic), two structurally coherent terranes (Taysanlı/Turkey; Alpine Corsica/France), and the eclogite blocks of the Pinchi Lake/Canada complex. Bulk major and TE compositions were also determined for lawsonite-bearing host rocks to understand petrogenesis and assess compositional evolution. Most analyzed mélange and coherent-terrane metabasalts have normal mid-ocean ridge/back-arc basin basalt signatures and they preserve compositional $evidence\ supporting\ interactions\ with\ (meta) sediment\ \pm\ metagabbro/serpentinite\ (e.g.\ LILE/LREE\ enrichments).$ Most lawsonite grains analyzed are compositionally zoned in transition-metal elements (Fe, Ti, Cr), other TEs (e.g. Sr, Pb), and/or REE, with some grains showing compositional variations that correlate with zoning patterns (e.g. Ti-sector zoning, core-to-rim zoning in Fe, Cr-oscillatory zoning). Our results suggest that compositional variations in lawsonite formed in response to crystallographic control (in Ti-sector zoning), fluid-host rock interactions, modal changes in minerals, and/or element fractionation with coexisting minerals that compete for TEs (e.g. epidote, titanite). The Cr/V and Sr/Pb ratios of lawsonite are useful to track the compositional influence of serpentinite/metagabbro (high Cr/V) and quartz-rich (meta)sediment (low Sr/Pb). Therefore, lawsonite trace and rare earth element compositions effectively record element redistribution driven by metamorphic reactions and fluid-rock interactions that occurred in subduction systems.

Keywords: lawsonite, metasomatism, metamorphism, subduction, fluid

INTRODUCTION

The slab-mantle interface in subduction zones is a locus of fluid-rock interactions, with considerable consequences for geochemical processes. Dehydration reactions occur over a range of pressure and temperature conditions and release fluids from subducted slabs (Schmidt & Poli, 1998; Hacker et al., 2003; van Keken et al., 2011; Muñoz-Montecinos et al., 2021). The liberated fluids transfer incompatible elements (e.g. large ion lithophile elements (LILE)) into the overlying mantle (You et al., 1996; Elliott, 2003), and at depths >100 km in most subduction zones, induce flux melting in the mantle to generate arc magmas (Tatsumi et al., 1986; Tatsumi & Eggins, 1995).

An abundant hydrous mineral in the crustal part of many subduction zones is lawsonite, a Ca-Al silicate $[CaAl_2Si_2O_7(OH)_2\cdot H_2O]$ that is a major host of transition metal elements (e.g. Cr, Fe, Ti), trace elements (TE; e.g. Sr,

Pb, U, Th, and rare earth elements (REE)) (Spandler et al., 2003; Usui et al., 2007; Martin et al., 2011, 2014; Vitale Brovarone et al., 2014; Hara et al., 2018; Fornash et al., 2019; Muñoz-Montecinos et al., 2021), and H₂O (up to 11.5 wt%). Since lawsonite is stable from forearc to subarc depths (Pawley, 1994; Poli & Schmidt, 1995; Schmidt & Poli, 1998; Forneris & Holloway, 2003), it serves as a vessel for H₂O and TEs in subduction zones. TEs in lawsonite show diverse zoning patterns depending on (1) reaction histories between lawsonite and coexisting minerals that compete for elements (e.g. epidote/allanite, apatite) (Spandler et al., 2003; Martin et al., 2014; Fornash et al., 2019), (2) the element selectivity that differs for each growth plane of lawsonite (Ueno, 1999; Vitale Brovarone et al., 2014; Fornash et al., 2019), and (3) interactions with internally/externally derived fluids (Martin et al., 2014; Vitale Brovarone et al., 2014; Fornash et al., 2019). In addition, isotopic zoning preserved in lawsonite (e.g. Li, Sr, Pb) signals the timing of fluid-rock interactions and

^{*}Correspondingauthor: E-mail: kangx691@umn.edu

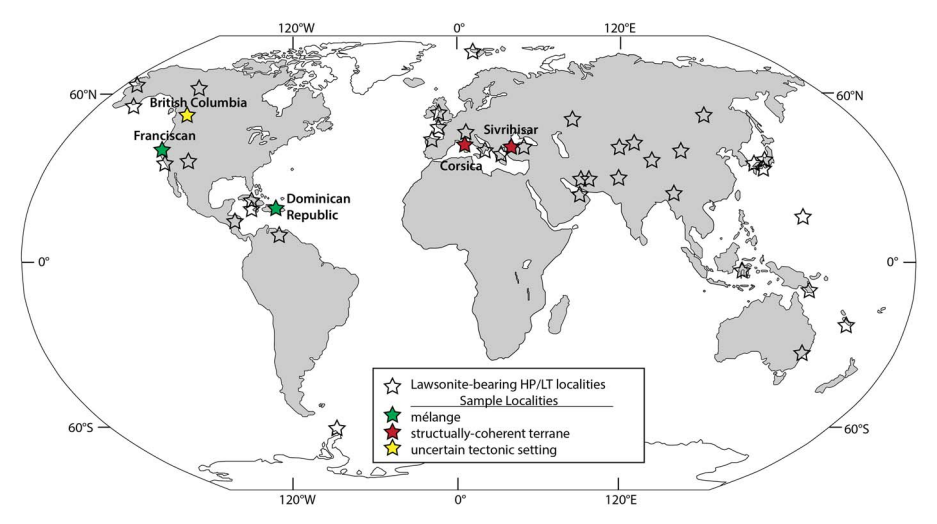


Fig. 1. Representative lawsonite-bearing locations, including sample locations for this study (modified from Whitney et al., 2020).

indicates the origin of host-rock protolith and the source of metasomatic fluids (Simons et al., 2010; Hara et al., 2018). In this respect, lawsonite is a significant phase that can monitor changes in various aspects of subduction systems.

The occurrences of HP/LT rocks can be characterized as tectonic blocks within mélange or as more structurally coherent complexes (Fig. 1). Examples of lawsonitebearing HP/LT rocks in mélange are Port Macquarie, Australia (Och et al., 2003; Nutman et al., 2013), the South Motagua Mélange Zone, Guatemala (Harlow et al., 2003; Endo et al., 2012) and the northern Rio San Juan Complex of the Dominican Republic (Giaramita & Sorensen, 1994; Krebs et al., 2008) (Fig. 1). Examples of mostly coherent complexes are in Alpine Corsica, France (Martin et al., 2011; Vitale Brovarone et al., 2014), the Tavşanlı Zone, Turkey (Davis & Whitney, 2006; Whitney et al., 2014; Fornash et al., 2019), the Zagros zone, Southern Iran (Agard et al., 2006; Angiboust et al., 2016), and the Sanbagawa belt, Japan (Tsuchiya & Hirajima, 2013) (Fig. 1). In some HP/LT terranes the field relations are uncertain; e.g. in the Pinchi Lake terrane, British Columbia, Canada, blueschist is structurally coherent but lawsonite eclogite occurs as blocks in glacial deposits (Ghent et al., 1993, 1996, 2009; Fig. 1).

In this study, we report the compositional record of lawsonite in HP/LT metamafic and metasomatic rocks from two mélanges (Franciscan/USA; Rio San Juan/Dominican Republic), two structurally coherent terranes (Tavşanlı/Turkey; Alpine Corsica/France), and the Pinchi Lake/Canada complex. TE compositions were obtained using laser ablation inductively coupled plasma-mass spectrometry (LA-ICP-MS), and the distribution of some TEs (e.g. Cr, Ti, Fe) was determined by X-ray mapping with an electron microprobe. This microanalytical approach can detect compositional variations that developed at different stages of metamorphic evolution in individual lawsonite grains. Bulk-rock compositions were also determined for lawsonite-bearing host rocks to understand petrogenesis and track compositional evolution. This

allows the evaluation of lawsonite and bulk-rock compositions to investigate elemental redistribution that occurred at different stages of metamorphism and metasomatism. Therefore, this study is relevant to understanding chemical processes driven by metamorphic reactions and fluid-rock interactions in subduction systems.

GEOLOGICAL BACKGROUND

Here we briefly review the field relationships and P-T histories of the five subduction complexes analyzed.

Mélange

Franciscan Complex, CA, USA

The Franciscan Complex of California developed by mid-Jurassic to Cretaceous subduction of the Farallon plate beneath the North American plate (Blake Jr., 1988; Wakabayashi, 1992; Ernst, 2011; Dumitru et al., 2013, 2015). It mostly comprises coherent thrust sheets of metabasaltic and metasedimentary rocks (Coleman & Lanphere, 1971; Blake Jr., 1988) and mélange units consisting of blocks within a serpentinite or siliciclastic matrix (Blake Jr., 1988; Wakabayashi, 1992; Wakabayashi et al., 1999).

Lawsonite-bearing HP/LT rocks occur primarily as blueschists (Platt, 1975; Wakabayashi & Dumitru, 2007; Wakabayashi, 2015). High-grade blocks in mélange evolved along an anticlockwise P-T path from epidoteamphibolite (600-700°C, 0.7-1 GPa) to epidote-eclogite (550-620°C, 2.2-2.5 GPa), through epidote-blueschist (300-400°C, 0.6-1 GPa), to lawsonite-blueschist facies conditions (150-250°C, 0.6-1 GPa) (Wakabayashi, 1990; Krogh et al., 1994; Ernst & Liu, 1998; Tsujimori et al., 2006; Page et al., 2007) (Fig. 2).

Rio San Juan Complex, Dominican Republic

The Rio San Juan Complex of the Dominican Republic formed during Mesozoic to Cenozoic convergence between the Caribbean intra-oceanic arc system and the North American continent (Pindell & Kennan, 2009;

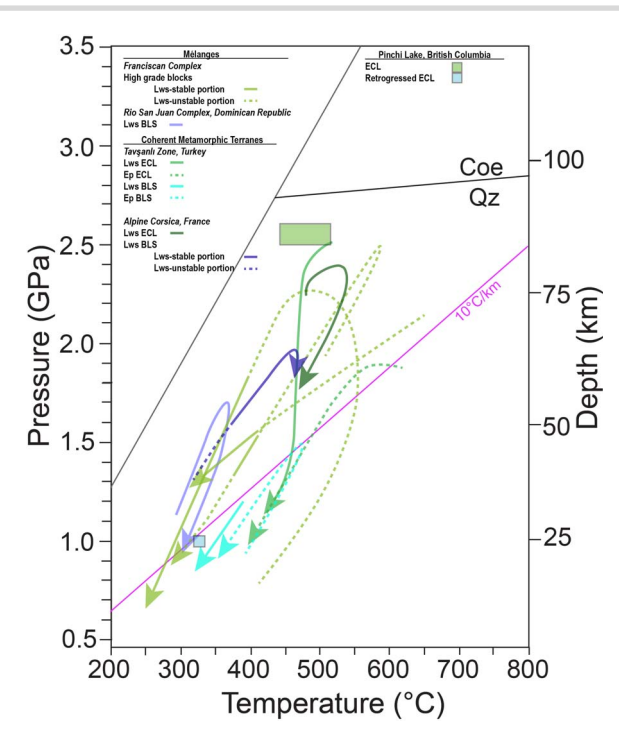


Fig. 2. P-T paths of lawsonite-bearing HP/LT rocks from Franciscan Complex/USA (Wakabayashi, 1990; Krogh et al., 1994; Ernst & Liu, 1998; Tsujimori et al., 2006; Page et al., 2007), Rio San Juan Complex/Dominican Republic (Krebs et al., 2011), Sivrihisar Massif/Turkey (Davis & Whitney, 2006; Pourteau et al., 2019), and Alpine Corsica/France (Vitale Brovarone et al., 2014). Blue and green rectangles indicate the prograde condition of retrogressed eclogite and the peak condition of eclogite from the Pinchi Lake/Canada, respectively (Ghent et al., 1993, 2009).

Escuder-Viruete et al., 2011, 2013). The northern part of the Rio San Juan complex consists of massive bodies of serpentinite, coherent bodies of greenschist-blueschist, and serpentinite-matrix mélanges. Mélange includes blocks of serpentinite, eclogite, blueschist, jadeitite, and marble, with the occurrence of lawsonite primarily confined to blueschist-facies rocks (Krebs et al., 2008, 2011).

Lawsonite blueschist evolved along a clockwise P-T path (Krebs et al., 2008, 2011) (Fig. 2). Peak conditions were 360–370°C and 1.6–1.7 GPa (Krebs et al., 2008, 2011) (Fig. 2). Lawsonite eclogite has only been reported in one region (Samaná Peninsula; Zack et al., 2004; Escuder-Viruete & Pérez-Estaún, 2006). This eclogite occurs as a boulder and has estimated peak conditions of 360°C and 1.6 GPa (Zack et al., 2004).

Structurally coherent terranes Sivrihisar Massif, Tavşanlı Zone, Turkey

The Tavşanlı Zone, Turkey, marks the subduction of passive continental margin and shallow marine sequences during Late Cretaceous convergence between the Anatolide-Tauride microcontinent and Eurasia (Okay & Kelley, 1994; Sherlock & Okay, 1999; Davis & Whitney, 2006; Okay & Whitney, 2010; Plunder et al., 2013; Fornash et al., 2016). The Sivrihisar Massif is located at the SE part of the Tavşanlı Zone and has excellent exposures of lawsonite eclogite (Davis & Whitney, 2006, 2008; Whitney & Davis, 2006; Okay & Whitney, 2010; Teyssier et al., 2010; Whitney et al., 2014). Lawsonite eclogite occurs as meters-scale pods within blueschist-facies metabasaltic and metasedimentary (calcschist, quartzite) units (Davis & Whitney, 2008; Whitney et al., 2014) or as mm- to dm-scale layers alternating with lawsonite blueschist (Davis & Whitney, 2006, 2008; Whitney & Davis, 2006; Teyssier et al., 2010; Whitney et al., 2014; Fornash et al., 2016, 2019). Within these structurally coherent units, serpentinite and metagabbro occur as rare pods or lenses (Çetinkaplan et al., 2008; Davis & Whitney, 2008; Whitney et al., 2014). Some meter-scale lenses of antigorite serpentinite are in contact with lawsonite + chloriterich (± garnet) metasomatic reaction zones (Plunder et al., 2013; Zack, 2013; Whitney et al., 2014; Fornash et al., 2019).

Lawsonite-bearing blueschist, eclogite, and interlayered blueschist/eclogite record a range of peak P-T conditions (380-570°C, 1.2-2.4 GPa) (Davis & Whitney, 2006, 2008; Kang et al., 2020) and there are indications of an anticlockwise P-T path (Davis & Whitney, 2006, 2008) (Fig. 2). Retrograde lawsonite blueschist records metamorphic conditions of ~450-500°C and ~1.5 GPa (Davis & Whitney, 2006, 2008).

Alpine Corsica, France

Alpine Corsica consists of a stack of nappes, including the Schistes Lustrés complex derived from oceanic successions with remnants of the ocean-continent transition (Waters, 1990; Molli et al., 2006; Vitale Brovarone et al., 2011a). Lawsonite-bearing HP/LT units are exposed in the Schistes Lustrés and show an increase in metamorphic grade structurally downward from blueschist (350–460°C, 1.5-1.8 GPa) to eclogite-facies units (490-550°C, 2.2-2.4 GPa) (Ravna et al., 2010; Martin et al., 2011; Vitale Brovarone et al., 2011b) (Fig. 2). Lawsonite-blueschist units differ from lawsonite-eclogite units in their higher proportions of metasedimentary vs. metaophiolitic sequences (Vitale Brovarone et al., 2011a; Meresse et al., 2012). In both units, lawsonite metasomatite formed along the lithological boundaries between metaophiolite and metasediment (Martin et al., 2011; Vitale Brovarone et al., 2011a, 2014).

Other field setting

Pinchi Lake, British Columbia, Canada

The Pinchi Fault Zone in central British Columbia marks a Permian-Triassic oceanic subduction zone (Paterson & Harakal, 1974; Paterson, 1977; Ghent et al., 1996). In the fault zone, a series of elongate units vary in lithology and metamorphic grade, including blueschist facies metasedimentary and metamafic rocks and serpentinized ultramafic rocks (Paterson, 1973, 1977).

Coherent blueschist units contain lawsonite and record a range of P-T (230-330°C, 0.8-1.2 GPa) (Paterson, 1973). Lawsonite-bearing eclogites are exposed at two different locations in the Pinchi Lake area (Paterson, 1977; Ghent et al., 1993, 2009). They occur as isolated

boulders without showing any clear geological context (Paterson & Harakal, 1974; Ghent et al., 1993, 2009). Despite the uncertain field relations, lawsonite eclogite boulders have been interpreted to be part of a mélange that is genetically associated with coherent blueschist units given their similarities in muscovite and phengite cooling ages (218 ± 7 Ma) (Paterson & Harakal, 1974; Ghent et al., 1996) and close proximity (Ghent et al., 1993, 2009). The least retrogressed eclogite has peak P-T conditions of 450°C and 2.5 GPa (Ghent et al., 2009), whereas more retrogressed eclogite records 310°C as a prograde T at a lower P limit of 1.0 GPa (Ghent et al., 1993) (Fig. 2).

PETROLOGY AND PETROGRAPHY

A summary of sample locations and modal mineralogy is provided in Table 1.

Franciscan Complex, CA, USA (mélange)

We analyzed four samples from two different serpentinitematrix mélanges (Ring Mountain and North Berkeley Hills) and one siliciclastic-matrix mélange (Blind Beach, Sonoma County).

Ring Mountain, Tiburon Peninsula, Marin County

The Ring Mountain mélange is known for the abundance of high-grade metabasaltic blocks (blueschist, eclogite, and amphibolite) within a serpentinite matrix (Coleman & Lanphere, 1971; Wakabayashi, 1992; Tsujimori et al., 2006). The mélange is structurally overlain by an ultramafic unit (Coleman & Lanphere, 1971; Wakabayashi, 1992; Tsujimori et al., 2006), and some high-grade blocks are partially encased by metasomatic actinolite-chloritetalc-phengite rinds (Coleman & Lanphere, 1971; Catlos, 2003). The two lawsonite-bearing samples analyzed from this locality were provided by S.R. Mulcahy: RR-1 (Mulcahy et al., 2014) and LVT-1.

Sample LVT-1 is a metabasalt comprised of omphaciterich and glaucophane-rich layers alternating at a mmto cm-scale (Fig. 3a). Both layers have the same mineral assemblage (garnet + omphacite + lawsonite + epidote + glaucophane + phengite + rutile, partially replaced by titanite + apatite with later chlorite + Fe-oxide) but differ in mode, and they contain a lawsonite-rich layer (vein) (Fig. 3a). In both blueschist and eclogite layers, lawsonite, phengite, glaucophane, and omphacite define the foliation (Fig. 3a), and garnet contains inclusions of epidote, omphacite, quartz \pm rutile \pm apatite \pm zircon. The lawsonite-rich layer (vein) is up to 4 mm thick, and it is concordant with the foliation.

Lawsonite in the lawsonite-rich layer is euhedral and significantly coarser than euhedral, matrix lawsonite (up to 2.8 mm vs. 90–520 μ m in length), thereby interpreted to have crystallized in situ in the vein (Fig. 3a and b). Partially chloritized garnet + omphacite + glaucophane + phengite + epidote + rutile (partially replaced by titanite) either crosscut or occur inside the vein (Fig. 3a and b).

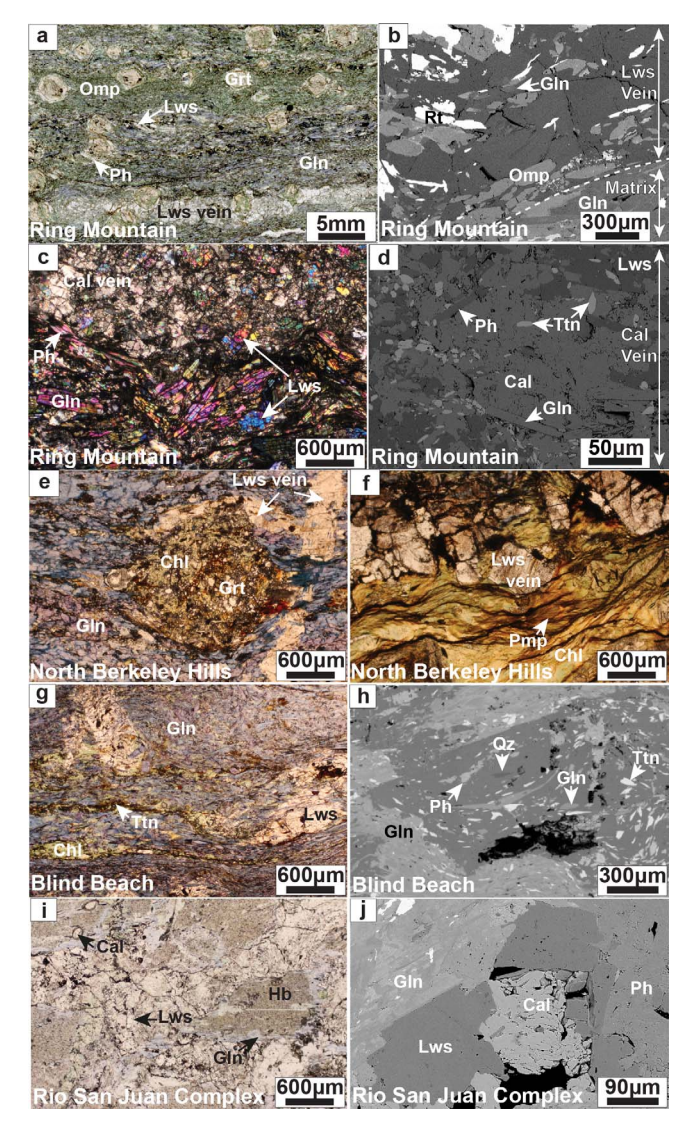


Fig. 3. Lawsonite-bearing samples from mélanges. (a, b) Images of interlayered metabasalt within the Ring Mt serpentinite-matrix mélange (LVT-1), showing alternating omphacite-rich and glaucophane-rich layers (a; PPL), and inclusions in lawsonite-rich layer (b; BSE). Dashed line indicates the boundary between the glaucophane-rich matrix and the lawsonite-rich layer (b; BSE). (c, d) Images of blueschist within the Ring Mt serpentinite-matrix mélange (RR-1), showing calcite vein (c; XPL) and inclusions in the vein (d; BSE). (e, f) Photomicrographs of blueschist from the North Berkeley Hills (EC-1B). Two different generations of lawsonite veins (e; PPL) show a partial-to-extensive replacement by chlorite and pumpellyite (f; PPL). (g, h) Images of blueschist within the siliciclastic-matrix mélange at Blind Beach (SM-8), showing matrix phases (g; PPL) and inclusions in lawsonite (h; BSE). (i, j) Images of blueschist-facies metagabbro exposed in the northern Rio San Juan Complex (IEC15-3.5), showing matrix minerals (i; PPL), and lawsonite partially replaced by calcite (j; BSE). Mineral abbreviations follow Whitney & Evans (2010).

Sample RR-1 is a lawsonite-blueschist, consisting of glaucophane, lawsonite, and phengite, with minor amounts of titanite and apatite (Fig. 3c). A calcite vein in the sample developed parallel to the foliation defined by the major matrix minerals (Fig. 3c). All matrix minerals are included in or crosscut the calcite vein (Fig. 3d). Lawsonite in the matrix and the vein are subhedral to euhedral (Fig. 3c and d) and commonly contain titanite.

Downloaded from https://academic.oup.com/petrology/article/63/8/egac065/6649808 by University of Minnesota - Twin Cities user on 31 August 2022

Table 1: Sample locations and mineral modal abundances

Sample	Location								Mine	ral moc	lal asbı	Mineral modal asbundance (%)	(%) e						
			Lws	Ep	Gln	Amp	Omp	Aug	Ph	Grt	Rt	Ttn	Qz	Ap	Chl	Pmp	Cal F	Fe-oxide	Zm
LVT-1	37°54′18.59′′N	Matrix (BLS)	6	56	30		13 ^G		20	6	ტ *∞	ı	ڻ ن	U.	m		m		ڻ ان
	122°29'32.46"W	Matrix (ECL)	10	99	14		28 ^G		18	10	£, 6, 6, 6, 6, 6, 6, 6, 6, 6, 6, 6, 6, 6,		_G	<1 ^G	2		2		ڻ ڻ
RR-1	37°54′19.67″N	Matrix	14		46				26			5 _L		1			7		
	122°29′29.16′′W	Cal-Vein	33		19				1			3^{L}		<1		Ì	43		
EC-1B	37°55′55.08″N	Matrix	22		41^{L}				∞	^	*	4		<<1 ^L	24				
	122°18'32.34"W	Chl + Pmp-rich area	26		∞				12			2+		<1+	50				
															(Chl + F	+Pmp)			
SM-8	38°25′34.75′′N 123°6′58.00′′W	Matrix	39		38^{L}				1^{L}			7L	J	1^{L}	15^{L}		V	<1	L
IEC15-3.5		Matrix	15	1	∞	62 (Hb)	ᆸ		2		2*L					T	9	<1	
SV08-283C	39°35′42.85″N 31°16′17.36″E	Matrix	14^{G}	19 ^L ,G	5 ^L ,G	8 (Act)	15^{G}		19^{G}	12	$1^{\mathrm{L,G}}$	2 ^G	2 ^{L,G}	<1 ^G	e				^ ! !
SV01-50A	39°36′0.72″N 31°15′20.58″E	Matrix (BLS)	41		32^{L}		4^{L}		9		14*	口		J	1	. 1	1		
		Cal-Vein (BLS)	23		13^{L}		L		1		*_	ı			16		39		
		Matrix (ECL)	36	2	13		33^{L}		^		13*	コ	J	Г					
		Cal-Vein (ECL)	22	9	\ 		11^{L}		^		10*		3^{L}	T	4	Ì	44		
SV01-75A	39°35′59.40′N 31°15′56.40″E	Matrix	17^{G}	$1^{L,G}$	34 ^L ,G				32	^	L,G	3 ^{L,G}	4^{L}	$1^{\mathrm{L,G}}$	9		2		L,G
TZ10-2.2C	39°43′22.28′′N 29°48′42.49″E	Matrix	39	2^{L}			3 <u>r</u>					5 _L		$<1^{L}$	51^{L}]	. 1	Π		<<1 ^L
C13		Matrix	47	1^{L}			32^{L}	15				1^{L}	J	$<1^{L}$	4	. 1			
BLR4	54°30′N 124′W	Matrix	17^{G}		52		ტ		16^{G}	9	7		8 _G						
BLR5	54°30′N 124′W	Matrix	18 ^G		41		17^{G}		10	9	2*G		36	2	1				

*Some rutile grains are partially replaced by titanite. ^GMinerals that occur as garnet inclusions. ^LMinerals that occur as lawsonite inclusions.

Lawsonite in the vein is fine-grained (60–240 μ m) relative to lawsonite in the matrix (250 μ m-1.6 mm).

North Berkeley Hills

Blocks of blueschist outcrop either on top of or within a serpentinite body that occupies the crestline of the North Berkeley Hills (Brothers, 1954; de Roever & Brothers, 1955). A blueschist block (sample EC-1B) exposed along Arlington Avenue in North Berkeley, CA, USA, has been considered as one such block, and it consists of lawsonite + glaucophane + phengite + titanite, with minor amounts of garnet (partially replaced by chlorite) + rutile (partially replaced by titanite) + apatite + pyrite (Fig. 3e). Lawsonite in the matrix is euhedral and fine-grained (260–300 μ m), and it contains apatite and glaucophane. Lawsonite veins are either concordant or discordant to the foliation defined by lawsonite, glaucophane, and phengite (Fig. 3e). Chlorite and pumpellyite are texturally later than other matrix phases and have partially to completely replaced vein-lawsonite (Fig. 3f).

Blind Beach, Sonoma County

At Blind Beach, prehnite-pumpellyite facies siliciclasticmatrix mélange hosts clasts and blocks of diverse lithologies, including serpentinite, clinopyroxenite, blueschist, and amphibolite, as well as prehnite-pumpellyite facies sandstone, chert, and basalt (Wakabayashi, 2015). One lawsonite-blueschist sample (SM-8) was collected from a block, and it consists of lawsonite, glaucophane, phengite, apatite, and titanite with texturally late chlorite and Fe-oxide (Fig. 3g). Lawsonite has a variable grain size (210 μ m-1.7 mm), with some coarse grains impinged by trails of glaucophane and titanite (Fig. 3g). Lawsonite is subhedral to euhedral and contains most matrix minerals as inclusions (Fig. 3h).

Rio San Juan Complex, Dominican Republic (mélange)

Sample IEC15-3.5 is from a blueschist facies metamafic boulder in the northern Rio San Juan Complex. Amphibole occurs as a major matrix phase (Table 1) and is very coarse-grained (2.6–5.8 mm). The sample contains lawsonite, phengite, and homblende rimmed by glaucophane, with rare epidote, rutile (partially replaced by titanite), and calcite (Fig. 3i). Lawsonite has a grain size of 120–410 μ m and commonly contains omphacite, rutile, pumpellyite, and albite. Some lawsonite grains are partially replaced by calcite and are therefore subhedral in shape (Fig 3j). Owing to the coarse-grained size of the matrix phases, we described this sample as a metagabbro. This sample was provided by S.M. Gordon from a field trip stop on the 2015 International Eclogite Conference (sample IEC15).

Tavşanlı Zone, Turkey (structurally coherent)

Lawsonite-bearing samples were collected from an eclogite pod (SV08-283C), an interlayered metabasalt (SV01-50A), a blueschist layer (SV01-75A), and a lawsonite + chlorite-rich metasomatic block (TZ10-2.2C). The SV samples are from the Halilbağı area of the Sivrihisar Massif and the TZ sample is from further west in the Tavsanlı Zone.

Sample SV08-283C is an eclogite, consisting of omphacite + garnet + lawsonite + epidote + phengite + glaucophane and minor amounts of quartz + apatite + rutile + titanite + zircon, with actinolite (partially replacing glaucophane) + chlorite as secondary phases (Fig. 4a). Garnet contains most matrix phases as inclusions. Matrix lawsonite is mostly euhedral (Fig. 4a and b) and has a grain size of 470–530 μ m. Some lawsonite grains include epidote, glaucophane, quartz, and rutile (Fig. 4b).

SV01-50A comprises Sample glaucophane-rich (blueschist) and omphacite-rich (eclogite) layers alternating at a mm- to cm-scale (Fig. 4c). Both layers consist of lawsonite + glaucophane + omphacite + phengite + rutile (partially replaced by titanite) + texturally late chlorite but differ in mode (Fig. 4c). Epidote only occurs in eclogite layers (Fig. 4d). Calcite and quartz veins are in both layers and they either crosscut or are parallel to the foliation defined by lawsonite, glaucophane, and omphacite (Fig. 4c). Most matrix minerals are included in the calcite veins (Fig. 4d). Lawsonite is fine-grained (50-270 μ m) and euhedral in both the matrix and the vein. Lawsonite commonly includes glaucophane, omphacite, quartz, apatite, titanite, and pumpellyite.

Sample SV01-75A is from an extensive (tens of meters in outcrop) blueschist layer and consists of lawsonite + phengite + glaucophane + garnet and minor amounts of quartz + epidote + titanite + apatite (Fig. 4e), with texturally late chlorite and quartz and calcite veins. Lawsonite and garnet contain glaucophane, epidote, apatite, rutile, titanite, and zircon as inclusions (Fig. 4f). In addition, garnet includes lawsonite. Lawsonite is euhedral in shape and variable in grain size (190 μ m to 1.5 mm) (Fig. 4e and f).

Sample TZ10-2.2C is from a metasomatic zone located adjacent to a serpentinite lens (Plunder et al., 2013; Zack, 2013; Whitney et al., 2014; Fornash et al., 2019). It consists of subhedral to euhedral coarse-grained lawsonite (>0.5 mm) in a chlorite-rich matrix with minor amounts of omphacite, epidote, titanite, apatite, and zircon (Fig. 4g). Lawsonite contains epidote, aegirineaugite, titanite, apatite, zircon, pumpellyite, and Fe-oxide as inclusions. The sample site is near stop 2.2 in the field guide of Okay & Whitney (2010).

Alpine Corsica, France (structurally coherent)

In Alpine Corsica, lawsonite-bearing omphacitite has been found as mm- to cm-scale veinlets in blueschistfacies metagabbro (Vitale Brovarone, 2013). Omphacititehosting metagabbro typically occurs as blocks in metersscale metasedimentary sequences (e.g. quartzite, calcschist, marble) (Vitale Brovarone, 2013) and they are in proximity to metaophiolitic blocks (Lagabrielle & Lemoine, 1997).

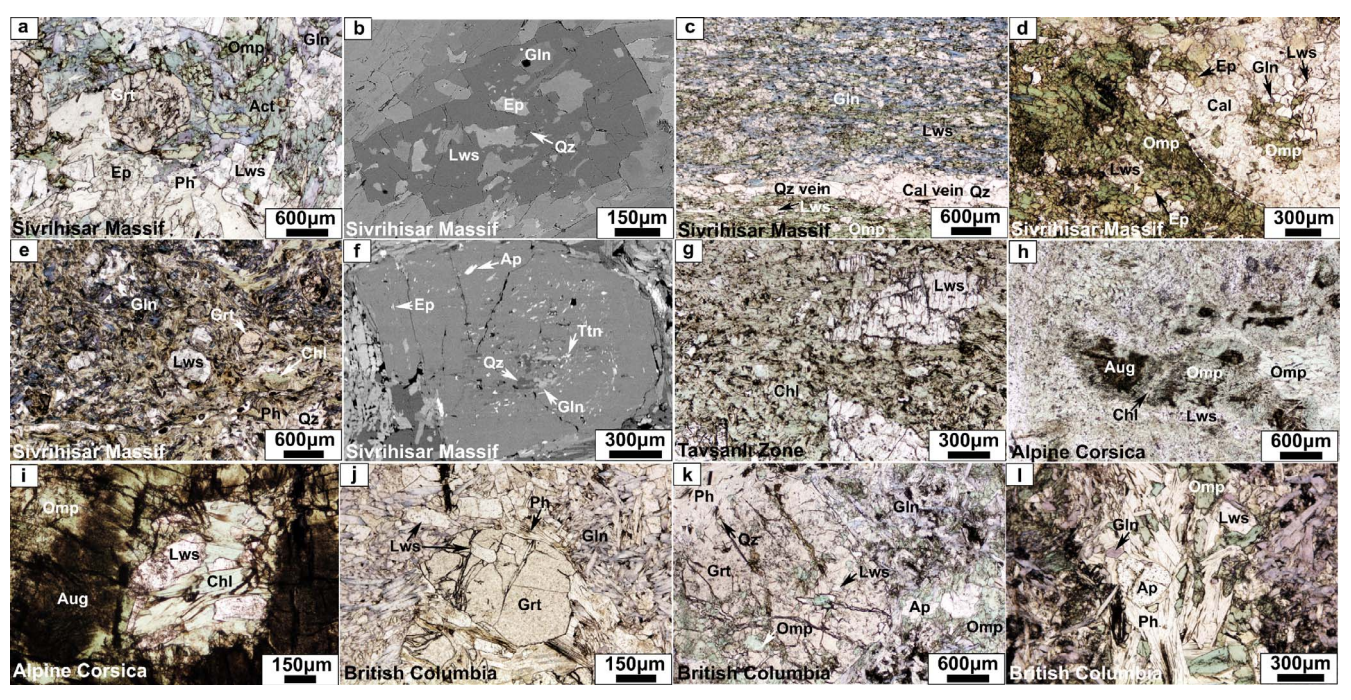


Fig. 4. Lawsonite-bearing samples from structurally coherent terranes. (a, b) Images of eclogite in the Sivrihisar Massif (SV08-283C), showing matrix phases (a; PPL) and inclusions in lawsonite (b; BSE). (c, d) Photomicrographs of Sivrihisar metabasalt, consisting of alternating blueschist and eclogite layers. Both blueschist and eclogite layers contain lawsonite in the matrix (c; PPL) and in the calcite vein (d; PPL). White dashed line indicates the boundary between the vein and the eclogite matrix (d). (e, f) Images of blueschist in the Sivrihisar Massif (PPL; SV01-75A), showing matrix phases (e; PPL) and inclusions in lawsonite (f; BSE). (g) Image of lawsonite + chlorite-rich metasomatite in the Tavşanlı Zone (PPL; TZ10-2.2C). (h, i) Photomicrographs of omphacitie-hosting metagabbro in Alpine Corsica (C13). Coarse-grained omphacite preserves relict augite (h; PPL), with partially dissolved areas filled with lawsonite + chlorite (i; PPL). (j) Photomicrograph of retrogressed eclogite from the Pinchi Lake, Canada (PPL; BLR4). (k, l) Photomicrographs of eclogite from the Pinchi Lake (BLR5), showing matrix phases (k; PPL) and lawsonite included in a phengite-rich area (I; PPL).

Sample C13 is an omphacitite-hosting metagabbro block exposed in a landslide. It mainly consists of omphacite and lawsonite with lesser amounts of epidote, titanite, and apatite (Fig. 4h). Coarse-grained omphacite (up to ~0.6 cm) has been boudinaged and preserves relict augite in the grain (Fig. 4h). Some omphacite grains are partially dissolved and filled with chlorite \pm omphacite ± lawsonite aggregates (Fig. 4i). Lawsonite is euhedral and has a grain size of 190–540 μ m. Omphacite, epidote, apatite, titanite, quartz, and pumpellyite occur as inclusions in lawsonite. The absence of key minerals (e.g. garnet, glaucophane) and unclear field relations (a landslide sample) make it hard to assign metamorphic facies for the sample. Therefore, the sample is referred to as a lawsonite-omphacite metagabbro (Lws-Omp metagabbro) in this study. The sample was provided by A. Vitale Brovarone.

Pinchi Lake, British Columbia, Canada (eclogite blocks)

Both samples (BLR4, 5) are from the Beaver Lake Road area, where eclogite blocks occur with glacial deposits. Sample BLR4 is a retrogressed eclogite, consisting of garnet, glaucophane, phengite, and lawsonite, with lesser amounts of rutile and quartz (Fig. 4j). Talc was reported in this sample by Ghent et al. (1993) but was not observed in the thin section analyzed.

Sample BLR5 is an eclogite, composed of garnet + omphacite + glaucophane + phengite + lawsonite + titanite + rutile (partially rimmed by titanite) + quartz + apatite with secondary chlorite (Fig. 4k). Some lawsonite grains in BLR5 are included in texturally later phengiterich areas (Fig. 41). Garnet in BLR4 has an inclusion assemblage (omphacite + lawsonite + phengite) slightly different from that in BLR5 (omphacite +lawsonite + quartz ± rutile; Fig. 4k). In both samples, matrix lawsonite is euhedral and has a grain size similar to or coarser than lawsonite inclusion in garnet (50–560 μ m vs. 51–280 μ m). The samples were collected by E.D. Ghent.

ANALYTICAL METHODS

Bulk-rock compositions of vein-excluding matrix areas were determined for the samples from mélange areas in the Franciscan (three samples: LVT-1, RR-1, EC-1B) and Rio San Juan Complex (one sample: IEC15-3.5), and from structurally coherent terranes in the Tavşanlı Zone (three samples: SV08-283C, SV01-75A, TZ10-2.2C) and Alpine Corsica (one sample: C13). We additionally analyzed the bulk-rock compositions of vein areas in two Franciscan blueschists (RR-1, EC-1B). Bulk major-element compositions were determined by X-Ray Fluorescence and selected TEs were measured by ICP-MS at the GeoAnalytical Lab at Washington State University (Table 2). Bulkrock major element compositions were calculated for the Pinchi Lake/British Columbia eclogites (BLR4, 5), using mineral modes and compositions because we only have thin sections of these two samples. To determine mineral

modes, Energy-dispersive X-ray spectroscopy mapping analyses were performed for selected areas within thin

Major- and minor-element compositions of minerals as well as X-ray element maps of lawsonite and garnet were acquired with a JEOL JXA-8530F Plus Electron Probe Microanalyzer in the Department of Earth and Environmental Sciences at the University of Minnesota. The in situ TE compositions of lawsonite, garnet, and apatite were measured using a Resonetics M-50 193 nm ArF excimer laser ablation system coupled to an Agilent 7700s quadrupole ICP-MS at the GeoHistory Facility, Curtin University. Details of analytical methods are presented in the Supplementary Material 1.

RESULTS

We present bulk-rock compositions (Table 2) as well as lawsonite, garnet, and apatite compositions (Tables 3 and 4; Supplementary Table S1). The compositions of other matrix minerals are presented in Supplementary Table S1.

Bulk-rock compositions

Metabasites from mélange and coherent-metamorphic

Mafic samples analyzed are considered as metabasalt and metagabbro (inferred to have a metavolcanic and plutonic protolith, respectively). In most cases this designation is based on grain size: coarse-grained samples are inferred metagabbro, although grain size in a metamorphic rock in some cases may not relate to grain size in the protolith owing to the effects of deformation and metamorphic reactions (e.g. Kang et al., 2020). Nevertheless, in cases in which a volcanic or plutonic protolith has been interpreted by others who have collected and/or studied the samples, we use these previously determined designations.

Analyzed metabasalt shows variable enrichment and/or depletion relative to normal mid-ocean ridge basalt (N-MORB; Gale et al., 2013) in terms of Al₂O₃ (12.1-18.7 wt%), MgO (3.38-9.26 wt), CaO (5.41-15.5 wt%), and P₂O₅ (0.11–1.62 wt%) with higher MnO (0.17–0.29 wt%) and K_2O (0.35–2.4 wt%) (Fig. 5; Table 2). As compared with the metabasalts from mélange areas, those from coherent-metamorphic terranes are lower in TiO₂, FeO_{tot}, and Na₂O (Fig. 5; Table 2). Metagabbro samples have bulk-rock compositions mostly within the range of these metabasalts, except for a few oxides; lower MnO in the Rio San Juan blueschist-facies metagabbro (IEC15-3.5; mélange), and higher Na₂O as well as lower TiO₂, FeO_{tot}, K_2O , and P_2O_5 in the Corsica Lws-Omp metagabbro (C13; coherent-terrane) (Fig. 5; Table 2).

Analyzed metabasalt samples are variably enriched and/or depleted in bulk V, Cr, and Ni with respect to N-MORB (174–366 μ g/g V, 82.5–443 μ g/g Cr, 57.7–323 μ g/g Ni; Fig. 5; Table 2). The highest Ni and Cr concentrations

were measured from the Sivrihisar blueschist (SV01-75A; coherent-terrane). Metagabbro samples have V, Cr, and Ni concentrations mostly within the range of the metabasalts, except the Corsica Lws-Omp metagabbro (C13; coherent-terrane) that has lower Cr and Ni contents.

Chondrite-normalized REE patterns of metabasalt samples are nearly flat-to-positively sloped (La/Yb_N = 0.85–12.1; N = Chondrite-normalized) (Fig. 6a). Primitive mantle (PM)-normalized TE patterns of these metabasalts display enrichments in LILE (e.g. Cs, Rb, and Ba) (Fig. 6b). Pb and Sr behave nonuniformly relative to the associated LREE; the coherent metabasalts show a positive Pb anomaly and a flat-to-negative Sr anomaly, whereas most mélange metabasalts show slight-tosignificant depletions in Pb and Sr, except for the Ring Mt blueschist/eclogite (LVT-1; mélange) with a positive Pb anomaly and the Ring Mt blueschist (RR-1; mélange) with a positive Sr anomaly (Fig. 6b).

The Rio San Juan blueschist-facies metagabbro (IEC15-3.5; mélange) shows a TE pattern similar to the metabasalts, and it is characterized by LREE, LILE and Sr enrichments with a negative Pb anomaly (Fig. 6). The Corsica Lws-Omp metagabbro (C13) has a distinct TE pattern with positive Pb and Sr anomalies and significant depletions in LREE (La/Yb_N = 0.58) and LILE as compared with the other metabasite samples (Fig. 6).

Metabasalt from Pinchi Lake, British Columbia

Retrogressed eclogite (BLR4) is depleted in TiO₂, FeO_{tot}, CaO, and Na₂O, but enriched in SiO₂, MgO, and K₂O relative to eclogite (BLR5) (Fig. 5; Table 2). The Cr content of BLR4, calculated from bulk Cr₂O₃, is higher than that of BLR5 (Fig. 5; Table 2). Despite the different degree of retrogression, both eclogite samples show significant enrichments in SiO₂ (54.5–58.3 vs. 42.2–52.0 wt%) and Na₂O (3.79–4.48 vs. 1.62–3.96 wt%) as compared with the other metabasite samples (Fig. 5; Table 2).

Metasomatite and lawsonite-bearing veins

Tavşanlı metasomatite (TZ10-2.2C; coherent-terrane) is significantly low in SiO2, Na2O and K2O, but high in Al₂O₃, FeO_{tot}, MnO, MgO, and V relative to the metabasite samples (Fig. 5; Table 2). The TiO₂, CaO, P₂O₅, Cr, and Ni contents of metasomatite are within the compositional ranges of the metabasites (Fig. 5; Table 2). The REE and TE patterns of Tavşanlı metasomatite are largely similar to those of the Sivrihisar metabasalts (SV01-75A, SV08-283C), showing LREE and Pb enrichments, with a negative Sr anomaly (Fig. 6). However, LILE content is significantly depleted in the metasomatite (Fig. 6b).

Lawsonite-bearing veins in two Franciscan mélange blueschists have compositions different from host blueschist matrix. In the North Berkeley Hills blueschist (EC-1B), the lawsonite vein is lower in SiO₂, TiO₂, Na₂O and K₂O, but higher in Al₂O₃, MgO and CaO relative to the host matrix (Fig. 5; Table 2). The bulk Ni and Cr concentrations of this vein is markedly higher than those

Table 2: Bulk-rock major and TE compositions

				Mélan	ge areas		C	Coherent me	etamorph	nic terrane	s		
Locality	Hills/Fr	Berkeley anciscan nplex	Ring M	ountain/Fra Complex	nciscan	Blind Beach/ Franciscan Complex	Rio San Juan Complex	Ta	vşanlı Zo	one	Alpine Corsica	Pinchi Lal Colui	
Rock type	BLS (Matrix)	BLS (Vein)	BLS (Matrix)	BLS (Vein)	BLS/ECL	BLS	BLS-facies Metagab- bro	BLS	ECL	Metaso- matite	Lws-Omp Metagab- bro	Retro- gressed ECL*	ECL*
Sample	EC-1B-M	EC-1B-R	RR-1-M	RR-1-V	LVT-1	SM-8	IEC15-3.5	SV01-75A	SV08- 283C	TZ10- 2.2C	C13	BLR4	BLR5
SiO ₂	49.3	44.3	42.2	39.0	49.2	48.4	48.5	52.0	43.7	30.8	48.6	58.3	54.5
TiO ₂	2.20	1.48	2.32	2.02	1.44	2.01	1.06	1.02	1.22	2.16	0.62	1.02	2.15
Al_2O_3	14.8	16.1	16.4	14.4	14.4	15.4	15.4	12.1	18.7	21.0	15.4	16.2	16.1
FeO _{tot}	12.4	12.5	6.62	6.22	9.38	11.9	8.14	8.09	7.70	14.0	6.10	7.71	8.61
MnO	0.19	0.26	0.19	0.15	0.22	0.23	0.16	0.17	0.29	0.30	0.18	0.15	0.14
MgO	5.96	8.98	3.38	3.12	8.04	5.96	7.77	9.26	4.26	13.8	6.16	7.18	6.40
CaO	5.41	6.63	13.5	16.5	8.96	6.73	10.2	5.67	15.5	7.51	14.5	4.07	6.52
Na ₂ O	3.68	2.31	2.51	2.33	3.47	3.94	2.91	2.35	1.62	b.d.l.	3.96	3.79	4.48
K ₂ O	1.39	0.36	2.40	3.02	1.47	0.35	0.92	1.91	1.50	< 0.01	< 0.01	1.54	1.10
P ₂ O ₅	0.25	0.12	0.59	0.52	0.11	0.18	0.08	0.14	1.62	0.53	0.02		
LOI Sum μg/g	4.07 95.5	6.48 93.0	9.28 90.2	12.3 87.3	2.75 96.7	4.66 95.1	4.33 95.2	6.99 92.7	3.61 96.1	9.73 90.0	4.20 95.6	100	100
μg/g La	8.30	4.87	34.6	39.0	8.90	5.27	4.85	17.6	50.7	56.6	1.52		
Ce	23.5	12.4	64.6	77.5	20.9	14.0	10.2	34.0	93.7	117	3.70		
Pr	3.80	2.10	7.50	9.28	2.87	2.47	1.60	4.24	11.9	14.0	0.72		
Nd	19.3	10.5	28.7	35.6	13.6	13.2	8.25	17.4	46.1	55.7	4.10		
Sm	6.21	3.38	5.73	7.42	4.10	4.51	2.90	4.32	9.92	13.3	1.69		
Eu	2.05	1.30	1.85	2.39	1.68	1.71	1.11	1.20	2.45	4.59	0.91		
Gd	7.78	4.50	5.43	6.74	5.27	6.38	3.85	4.57	9.52	14.1	2.53		
Tb	1.42	0.82	0.84	1.07	0.98	1.20	0.73	0.83	1.64	2.38	0.51		
Dy	8.81	5.27	4.75	5.90	6.29	8.03	4.76	5.32	10.3	14.7	3.39		
Но	1.81	1.11	0.95	1.12	1.26	1.74	1.02	1.05	2.12	3.01	0.75		
Er	4.84	3.09	2.39	2.89	3.31	4.83	2.85	2.80	5.75	8.27	2.08		
Tm	0.70	0.46	0.33	0.40	0.46	0.70	0.42	0.41	0.82	1.21	0.30		
Yb	4.50	2.79	2.05	2.46	2.89	4.47	2.60	2.44	5.11	7.79	1.88		
Lu	0.69	0.43	0.31	0.39	0.42	0.71	0.40	0.36	0.80	1.31	0.30		
Ba Th	196 0.54	91.1 0.48	636 5.24	445 5.98	898 0.90	97.0 0.29	222 1.02	150 3.29	232 14.4	4.39 21.2	8.79 0.08		
Nb	6.75	3.92	48.7	55.6	7.60	3.34	1.02	20.7	24.3	18.6	0.32		
Y	44.5	28.5	23.9	28.6	30.7	43.4	24.9	26.1	59.8	79.0	18.7		
Hf	5.03	2.68	5.12	5.91	2.55	3.43	1.84	3.33	6.23	9.95	0.86		
Ta	0.48	0.28	3.14	3.60	0.55	0.25	0.09	1.44	2.07	1.92	0.04		
U	0.22	0.21	0.84	1.07	0.72	0.37	0.18	0.71	3.94	3.20	0.04		
Pb	2.09	1.05	4.29	3.66	8.98	0.41	0.47	6.37	32.3	23.0	0.97		
Rb	30.3	7.72	59.6	48.0	37.4	8.24	15.9	50.4	38.1	0.22	0.39		
Cs	0.88	0.21	1.23	0.92	2.05	0.33	0.19	1.88	1.72	0.01	< 0.01		
Sr	52.3	58.7	648	480	188	38.5	164	128	817	755	126		
Sc	45.0	33.6	18.2	20.4	38.4	46.4	35.9	24.3	30.0	86.6	41.3		
V C	291	270	174	147	237	366	231	174	209	451	229	200	105
Cr	227	550	82.5	74.0	399	235	317	443	177	115	66.8	300	105
Ni 7-	84.1	331	57.7	52.3	194	77.1	71.5	323	71.1	58.3	45.4		
Zr	191	99.6	224	252	98.1	125	66.0	133	245	356	24.4		

 $FeO_{tot} = All\ iron\ is\ reported\ as\ FeO\ wt\%; LOI = H_2O\ determined\ from\ loss\ of\ ignition.\ ^*Bulk-rock\ compositions\ calculated\ from\ mineral\ modes\ and\ compositions.$

of the matrix with a minor difference in V content (Fig. 5; Table 2). In contrast, a lawsonite-bearing calcite vein in the Ring Mt blueschist (RR-1) is lower in concentrations for most major element oxides (except CaO and K2O), V, Cr, and Ni as compared with the matrix (Fig. 5; Table 2). These lawsonite-bearing veins generally follow the REE and TE patterns of the corresponding matrices but differ in REE abundances from the matrices; veins in EC-1B and RR-1 contain lower and higher REE contents, respectively (Fig. 6a).

Downloaded from https://academic.oup.com/petrology/article/63/8/egac065/6649808 by University of Minnesota - Twin Cities user on 31 August 2022

Table 3: Representative compositions and zoning patterns of lawsonite

		Fe	F	ប៉		Fe (wt%)	Ti (wt%)	ŭ	Sr	Pb	>	Sr/Pb	Cr/V	La/Dy _N	Dy/Yb _N	La/Yb _N
			Zoning Patterns	St										Normal	Normalized to chondrite	ndrite
<u>Mélanges</u> Ring Mountai LVT-1 (BLS/ECL)	Mélanges Ring Mountain, Franciscan Complex LVT-1 Matrix Lws Core to 1 (BLS/ECL) (BLS; Zone	Complex Core to rim	Hourglass- sector	N.D.	Min	0.57	90.0	319	243	2.60	347	93.6	0.92	0.40	0.26	0.10
	Matrix Lws (BLS; Zone				Max Avg Min	0.90	0.08	409 364 403	422 333 326	4.16 3.38 2.09	444 396 369	101 97.5 127	0.92 0.92 0.91	0.65 0.53 0.18	0.82 0.54 0.33	0.54 0.32 0.09
	Lws Vein (BLS; Zone	Hourglass- sector	Hourglass- sector	Irregular	Max Avg Min	0.52 0.34 0.49	0.05 0.02 0.11	483 441 1397	813 582 843	4.49 3.60 10.0	445 401 346	181 160 78.1	1.22 1.11 3.40	0.29 0.26 0.45	1.10 0.76 2.78	0.29 0.19 1.25
	²) Lws Vein (BLS; Zone 3)	S; Zone 3)			Max Avg Min Max Avø	0.56 0.49 0.42 0.70	0.16 0.13 0.01 0.07	1727 1530 473 1166 748	887 866 251 827 439	11.4 10.5 3.41 11.2 5.58	450 397 262 404	85.7 82.5 73.6 91.1	4.53 3.88 1.81 2.89	0.68 0.59 0.43 0.76	3.47 3.19 0.70 2.56	2.37 1.89 0.31 1.87
	Lws Vein (ECL; Zone 2) Lws Vein (ECL; Zone 3)	N.D.	Hourglass- sector	Irregular	Min Max Avg Min	0.70 0.70 0.53	0.06	397 745 587 559	273 273 336 658	3.04 4.41 4.03 7.09	303 303 333 498	61.9 110 84.1 92.8	2.30 2.30 1.78 1.06	0.86 0.86 0.07 0.25	0.15 0.75 0.45 0.19	0.12 0.65 0.06
RR-1 (BLS)	Matrix Lws Lws in Cal-Vein	Oscillatory Core to rim	Oscillatory Core to rim	N.D.	Max Avg Min Max Avg Mantle*	0.66 0.60 0.27 0.75 0.38	0.05 0.03 0.05 0.41 0.13	572 566 37.5 194 106 89.9	916 787 296 593 445 201	8.13 7.61 0.98 6.40 3.58 4.58	527 513 138 290 231 227	113 103 57.9 453 181 44.6	1.15 1.10 0.20 0.77 0.45 0.38	0.49 0.37 4.58 24.7 10.5 3.79	0.24 0.22 2.39 5.34 3.98	0.09 0.08 16.2 97.3 41.5 2.86
North Berkele EC-1B (BLS)	North Berkeley Hills, Franciscan Complex EC-1B (BLS) Matrix Lws Core to rim Lws Vein Core to rim	scan Complex Core to rim N.D. Core to rim Irregular	k N.D. Irregular	N.D. Core to rim	Rim* Avg Mantle* Rim* Avg Core* Rim*	0.41 0.32 1.04 1.17 0.98 1.13 1.14	0.21 0.03 0.05 0.05 0.19 0.11	158 117 303 87.7 333 876 1179 905	305 243 191 385 235 235 58.1 83.3 68.8	4.91 4.71 1.84 3.66 2.05 0.70 0.70	272 245 241 774 621 515 466	66.0 53.2 104 109 141 78.5 117	0.58 0.46 0.56 0.11 0.56 1.70 2.57	10.6 6.52 6.10 4.70 4.86 1.59 1.71	1.81 1.18 2.48 0.48 0.78 0.96	19.4 9.47 12.2 2.24 9.57 0.71 1.35
																Continued

2.75 5.12 11.7

1.07 2.07 4.64

2.55 2.31 2.52

1.12 0.95 0.65

34.8 26.6 17.2

511 450 291

8.50 7.45 6.75

294 206 116

568 435 188

0.04 0.12 0.19

0.94 0.81 0.80

Avg Core*

N.D.

Matrix Lws Core to rim Irregular (ECL)

Rim*

(BLS)

SV01-50A (BLS/ECL)

Continued

8.26

1.52 2.17

0.18

49.8

328

8.05

401

60.6

0.05

1.09

Rim*

Downloaded from https://academic.oup.com/petrology/article/63/8/egac065/6649808 by University of Minnesota - Twin Cities user on 31 August 2022

Table 3: Continued	Continued															
		Fe	Έ	ď		Fe (wt%)	Ti (wt%)	ď	Sr	Pb	>	Sr/Pb	Cr/V	La/Dy _N	Dy/Yb _N	La/Yb _N
			Zoning Patterns	ns										Norma	Normalized to chondrite	ndrite
	-	,														
Blind Beach SM-8 (BLS)	Blind Beach, Franciscan Complex SM-8 (BLS) Matrix Lws Core	implex Core to rim, Irregular	Irregular	Core to rim	Min	0.45	0.03	99.3	71.1	0.45	508	118	0.16	0.16	1.06	0.23
		Irregular				c	Ċ	C	, C	7	7	, C	L	C	7	Ċ
					Max Avg	2.09	0.38	284 192	103	1.14 0.80	560	138	0.36	0.30	1.44	0.32
Rio San Juar IEC15-3.5 (Metagab- bro)	Rio San Juan Complex, Dominican Republic IEC15-3.5 Matrix Lws Irregular Ir (Metagab-	ninican Repul Irregular	blic Irregular	N.D.	Min	0.12	0.02	7.70	323	0.63	46.9	184	0.14	0.37	0.86	0.45
					Max	0.70	0.24	92.0	682	2.05	241	1083	09.0	12.1	3.73	25.7
					Avg	0.30	0.08	33.2	546	1.28	121	518	0.28	5.47	1.99	11.6
Coherent A	Coherent Metamorphic Terranes	erranes)											
Sivrihisar IV SV08-283C	Sivrihisar Massif, Turkey SV08-283C Matrix Lws	Irregular	Irregular	N.D.	Min	06.0	0.03	190	97.7	25.9	302	30.6	0.53	0.92	4.92	5.76
					Max	1.74	0.28	424	1391	43.5	361	38.5	1.33	3.11	11.3	23.9
					Avg	1.15	0.11	300	1185	36.5	334	32.8	0.91	1.97	7.38	13.8
SV01-75A	Matrix Lws	Hourglass-	Hourglass-	Oscillatory	Min	1.02	0.03	338	514	11.0	332	46.7	1.02	0.89	1.92	2.00
(BLS)	(Zone 1)	sector, Oscillatory	sector													
					Max	2.04	0.67	354	879	15.1	348	58.1	1.02	1.04	2.82	2.52
					Avg	1.65	0.41	346	269	13.1	340	52.4	1.02	0.97	2.37	2.26
	Matrix Lws				Min	96.0	0.11	663	630	13.3	337	47.4	1.89	0.94	2.28	2.17
	(Zone 2)															
					Max	1.34	0.70	1003	702	13.7	350	51.3	2.98	0.97	2.32	2.22
					Avg	1.22	0.44	833	999	13.5	343	49.4	2.44	0.95	2.30	2.19
	Matrix Lws				Min	06:0	0.03	1134	1139	18.2	260	1.4	2.98	90.0	0.03	0.01
	(Zone 3)															
					Max	1.34	0.17	2020	2056	22.4	439	91.8	7.77	4.60	1.22	5.61
					Avg	96.0	0.03	1577	1598	20.3	349	46.6	5.37	2.33	0.63	2.81
	Matrix Lws				Min	06.0	0.02	1007	630	12.7	291	31.1	2.57	0.65	1.88	1.23
	(Zone 4)															
					Max	1.51	1.80	2456	1363	20.6	460	85.3	8.45	4.00	19.9	32.2
					Avg	1.24	0.62	1717	898	17.4	377	52.3	4.88	2.07	6.92	12.8
SV01-50A	Matrix Lws	Core to rim	Core to rim	Core to rim	Core*	0.57	0.22	373	102	6.19	402	16.5	0.93	2.75	6.29	17.3

Downloaded from https://academic.oup.com/petrology/article/63/8/egac065/6649808 by University of Minnesota - Twin Cities user on 31 August 2022

	Dy/Yb _N
	La/Dy_N
	Cr/V
	Sr/Pb
	Λ
	Pb
	Sr
	Cr
	Ti (wt%)
	Fe (wt%)
	ť
	ΪŢ
	Fe
le 3: Conunuea	
labi	

		Fe	F	ඊ		Fe (wt%)	Ti (wt%)	č	Sr	Pb	>	Sr/Pb	Cr/V	La/Dy _N	Dy/Yb _N	La/Yb _N
			Zoning Patterns	JS										Normal	Normalized to chondrite	ndrite
L'I	Lws in Cal-vein (BLS)	Core to rim	Core to rim	Core to rim	Core*	0.73	0.36	124	114	7.51	405	15.1	0.31	2.78	1.74	4.84
					Rim*	2.23	0.20	1055	215	4.99	331	44.6	3.39	5.41	1.27	7.14
		,	,	,	Avg	1.40	0.20	613	177	2.90	399	32.8	1.87	4.19	1.49	6.10
<u> й Ü Ш</u>	Lws in Cal-vein (ECL)	Irregular	Irregular	Irregular	Min	0.72	0.03	28.4	237	5.76	305	41.1	0.08	2.44	1.63	4.46
					Max	1.61	0.14	284	276	10.6	373	73.5	0.76	6.16	2.46	15.2
					Avg	1.01	0.07	150	454	7.97	350	55.9	0.42	4.42	2.01	80.6
TZ10-2.2C M (Metaso- matite)	Matrix Lws	Core to rim, Oscillatory, Irregular	Irregular	N.D.	Min	0.69	0.02	98.3	976	19.4	755	40.6	0.07	0.38	0.12	0.09
					Max	1.18	0.49	344	2830	53.2	1800	55.1	0.36	2.27	2.79	1.95
					Avg	0.97	0.18	176	1784	36.8	1210	48.5	0.16	0.98	0.97	0.81
Alpine Corsica, France	France															
C13 M (Metagab- bro)	Matrix Lws	Core to rim	Core to rim	N.D.	Core*	0.87	0.02	b.d.1.	969	1.72	1047	347	b.d.1.	0.77	1.39	1.07
					Rim*	0.59	0.03	3.80	610	0.94	1120	750	b.d.1.	0.88	1.16	1.00
					Avg	0.71	0.03	1.90	546	1.10	1085	577	b.d.1.	0.83	1.39	1.13
L	Lws in Cpx	Core to rim	Hourglass-	N.D.	Min	69.0	0.02	b.d.1.	184	0.00	122	Pb b.d.l.	Cr b.d.1.	0.33	0.92	0.34
Z)	(Zone 1)		sector				0		C		0				,	7
					Max	0.74	0.03	b.d.1.	283	2.20		Pb b.a.I.	Cr b.a.1.	0.44	T.03	0.41
					Avg	0.71	0.02	b.d.I.	234	1.10		Pb b.d.l.	Cr b.d.l.	0.39	0.98	0.37
(Z	Lws in Cpx (Zone 2)				Min	0.63	0.04	b.d.1.	160	b.d.].	113	Pb b.d.l.	Cr b.d.l.	0.30	0.45	0.28
					Max	92.0	0.05	b.d.1.	165	b.d.l.	127	Pb b.d.l.	Cr b.d.l.	0.67	0.93	0.30
					Avg	69.0	0.05	b.d.1.	162	b.d.l.	120	Pb b.d.l.	Cr b.d.l.	0.49	0.69	0.29
L	Lws in Cpx				Min	0.77	0.00	b.d.l.	300	b.d.l.	131	Pb b.d.l.	Cr b.d.l.	0.49	0.15	0.08
7)	(c alloz)				Max	0.87	0.00	ן לי	426	0.48	155	Ph h d 1	(r h d]	0.70	0.23	0.12
					Avo	 	10.0) hdl	373	0.18		Ph h d 1	Crhdl	0.56	0 1 0	0.10
Pinchi Lake, British Columbia	tish Colum	ıbia			9	0	H)	;	ì	9					9	9
BLR4 (Retro- Lws in Grt gressed ECL)	ws in Grt	Irregular	Core to rim, Irregular Irregular	Irregular	Min	0.16	0.02	616	202	1.10	74.0	184	7.25	2.76	0.69	1.89
					Max Avg	0.52	0.32	649	394	1.40	85.0	281	8.77	4.08	1.37	5.57
																Continued

1.03 73.4 74.3

1.35

469 403

47.8 62.2

0.94 270 629 2.21

1085 1.90 0.08

b.d.1.

25.3 1210 176

54.3 48.7

3.49 334 300 0.06

48.4 81.8 154

0.65

14.7 475 206 10.2

2.65 357 1238 3.42

121 33.2 4.84

8.08 231 106 7.88

b.d.l. b.d.l. 112 b.d.1.

143

348

92.1

70.5 16.0

Downloaded from https://academic.oup.com/petrology/article/63/8/egac065/6649808 by University of Minnesota - Twin Cities user on 31 August 2022

 La/Yb_N Normalized to chondrite Dy/Yb_N 3.12 6.71 1.06 0.91 0.86 3.62 1.69 4.73 4.88 4.64 641 La/Dy_N 3.68 8.43 2.13 18.3 11.3 19.3 4.49 Cr/∖ 3.08 2.38 1.87 1.21 1.31 0.32 0.29 740 16.9 49.4 63.0 121 54.2 33.9 50.3 546 76.4 148 111 147 181 359 210 270 264 568 469 579 1784 477 400 426 433 62.7 > 33.9 18.5 13.3 0.33 11.2 6.78 3.80 9.99 5.80 5.68 9.36 2.49 1185 689 982 452 740 796 582 708 483 641 379 606 514 Š 193 437 629 823 522 491 198 403 838 119 343 4.38 ប៊ Ti (wt%) 0.07 0.19 0.07 0.09 0.07 0.02 0.30 0.08 0.04 0.37 939 Fe (wt%) 0.27 0.30 0.50 0.50 0.50 69.0 0.20 0.51 0.49 0.69 0.34 546 Avg Mantle* Avg 78.1 Avg Mantle* Core* Rim* Rim* Rim* Avg Min Max Core to rim, Core to rim Core to rim Oscillatory, Irregular 499 2.10 399 415 0.03 Irregular ö Zoning Patterns Core to rim, Core to rim Core to rim, Irregular Irregular Irregular F Core to rim, Core to rim, Oscillatory Oscillatory, Irregular rregular Irregular Matrix Lws Matrix Lws Lws in Grt 235 8.50 621 333 2.04 Ph-vein Lws in BLR5 (ECL) Sr Sc < Sr Zr

Table 3: Continued

240

127

3.01 2.57 2.91

Concentrations are reported in $\mu g/g$ unless otherwise indicated; b.d.l. = below than detection limit (i.e. analyzed but not detected). *The average compositions of lawsonite with Fe-concentric zoning at core, mantle, and rim.

Downloaded from https://academic.oup.com/petrology/article/63/8/egac065/6649808 by University of Minnesota - Twin Cities user on 31 August 2022

Table 4: Average TE concentrations of lawsonite, garnet, and apatite in the matrix

			Mélan	Mélange areas				Cohe	Coherent metamorphic terranes	orphic terr	ranes					
Locality	North Berkeley Hills/Franciscan Complex	erkeley nciscan plex	Ring M Frand Con	Ring Mountain/ Franciscan Complex	Blind Beach/ Franciscan Complex	Rio San Juan Complex		H	Tavşanlı Zone	a)		Alpine Corsica	Pir	Pinchi Lake/British Columbia	itish Colun	nbia
Rock type	STR	δί	BLS	BLS/ECL	BLS	BLS-facies Metagabbro	BLS	Ω	EC	ECL	Metaso- matite	Lws-Omp Metagabbro	Retrogressed ECL	ssed ECL	ш	ECL
Sample	EC-1B	.1B	RR-1	LVT-1	SM-8	IEC15-3.5	SV01–75A	-75A	SV08	SV08-283C	TZ10-2.2C	C13	BLR4	34	В	BLR5
Mineral	Lws	Ap	Lws	Lws	Lws	Lws	Lws	Grt	Lws	Grt	Lws	Lws	Lws	Grt	Lws	Grt
La	20.4	5.20	69.4	1.00	3.24	26.8	7.78	60.0	9.07	0.01	5.20	2.66	54.9	60.0	28.9	0.04
Ce	62.6	17.0	146	3.04	11.0	56.7	19.4	0.23	21.3	90.0	13.3	7.45	124.2	0.19	57.2	0.15
Pr	10.7	5.40	16.9	0.50	2.22	7.03	2.63	0.02	2.88	b.d.l.	1.86	1.22	15.3	0.02	6.59	0.02
Nd	60.3	42.8	67.5	2.98	14.0	32.2	12.8	0.27	13.5	0.03	9.58	6.90	68.3	0.19	26.3	0.25
Sm	18.6	31.6	14.2	1.18	6.19	7.86	3.69	b.d.l.	3.62	b.d.l.	3.56	2.39	16.2	1.93	5.75	1.98
Eu	3.79	33.0	6.13	0.41	2.40	3.02	1.24	90.0	0.84	b.d.1.	1.44	1.36	3.89	2.20	1.86	2.00
Cd	19.5	194	11.7	2.15	9.23	7.75	4.61	99.0	4.82	0.14	6.41	3.22	11.6	20.4	5.26	12.5
Tb	2.50	50.4	1.61	0.43	1.67	0.97	69.0	0.45	0.79	0.11	1.03	0.50	1.21	8.14	0.78	1.9
Dy	12.5	453	8.69	3.79	11.8	5.31	4.33	9.25	5.89	3.23	7.34	3.54	2.67	75.0	5.17	9.43
Но	1.80	124	1.36	1.02	2.56	0.85	0.83	4.04	1.12	2.09	1.73	0.77	0.82	14.0	1.01	ij
Er	4.04	486	3.17	3.93	7.50	2.01	1.91	18.7	2.17	13.1	5.53	1.99	1.63	32.8	3.07	
Tm	0.49	8.06	0.30	0.64	1.09	0.24	0.21	3.46	0.15	3.13	0.83	0.26	0.18	3.87	0.47	0.51
Yb	2.78	540	1.59	4.60	7.23	1.44	1.04	23.8	0.49	28.4	6.57	1.74	1.17	19.9	3.00	3.33
Lu	0.36	91.4	0.19	0.81	1.25	0.18	0.12	3.45	0.04	4.62	1.36	0.29	0.15	2.17	0.46	0.52
Ва	5.66	00.00	28.1	0.24	2.35	30.4	2.51	0.79	0.34	1.45	3.00	0.27	18.9	0.26	17.52	0.07
Th	0.88	00.00	3.85	0.04	0.03	2.75	0.50	0.10	4.00	0.01	3.13	0.01	1.73	b.d.l.	1.49	b.d.1
Y	40.1	3678	38.5	29.0	62.9	22.2	23.1	116	33.2	67.5	51.4	19.4	23.0	392	30.0	44.3
JH	0.04	b.d.1.	0.27	b.d.1.	0.23	60.0	0.07	0.02	b.d.l.	0.17	0.70	b.d.1.	0.04	b.d.l.	b.d.1.	0.02
n	0.49	b.d.1.	1.13	b.d.1.	0.22	0.26	0.12	b.d.1.	0.44	0.03	0.58	b.d.1.	0.89	0.03	0.74	0.03
Pb	2.05	28.0	3.58	3.53	09.0	1.28	16.3	0.38	36.5	b.d.l.	36.8	1.10	33.9	0.26	6.78	0.26
Rh	0.61	b.d.1.	0.01	0.02	b.d.1.	1.84	69.0	0.28	b.d.1.	69.0	0.01	0.09	2.46	0.08	0.51	0.02

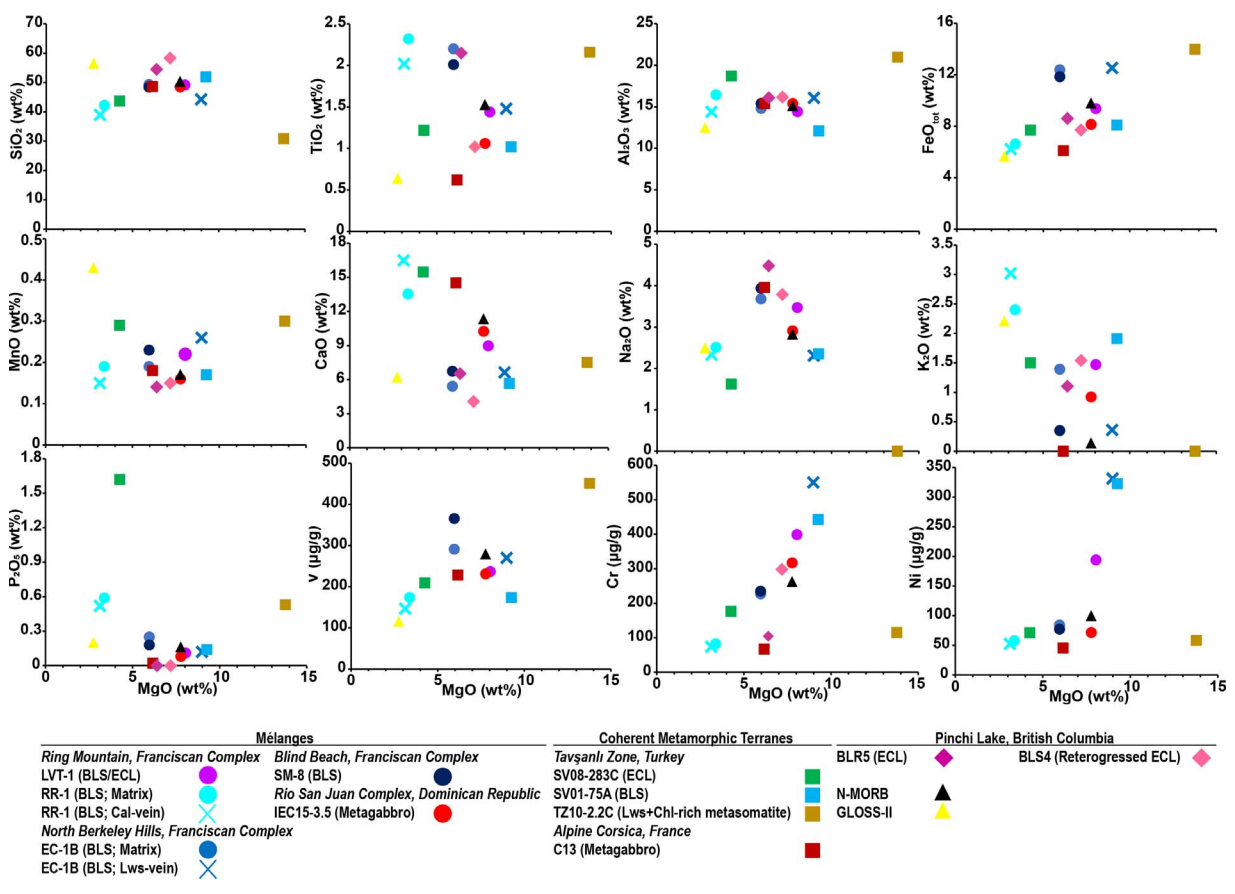


Fig. 5. Variation diagrams between MgO and other major and TEs (V, Cr, Ni). Also shown are N-MORB (Gale et al., 2013) and GLOSS-II (Plank, 2014) compositions.

Lawsonite composition

Lawsonite grains in various textural sites (i.e. garnet, matrix, and vein) with diverse textural features (e.g. included in the dissolved domains of omphacite) were analyzed in this study. Analyzed matrix grains are free of textural replacement, except a few grains replaced by calcite in the Rio San Juan blueschist-facies metagabbro (IEC15-3.5).

Transition-metal element compositions

Analyzed lawsonite contains detectable amounts of Cr and/or Ti, with Fe as the most common substituent (up to 2.9 wt% FeOtot) (Table 3; Supplementary Table S1). Fe content is negatively correlated with the sum of Al, Ti, and Cr contents when these elements are expressed in atoms per formula unit (Fig. 7). This negative correlation is lost when Ti or Cr is plotted against Al+Cr+Fe and Al + Ti + Fe, respectively. This confirms that Fe is the most common substituent for Al relative to Cr and Ti, and it is likely present as Fe³⁺. Most lawsonite grains have Cr and Ti contents <1 wt%, but in the Sivrihisar blueschist SV01-75A, Cr and Ti are incorporated at the weight percent level (\sim 1 wt% Cr₂O₃, \sim 3 wt% TiO₂) (Table 3; Supplementary Table S1).

Fe, Ti, and Cr zoning in lawsonite

Analyzed lawsonite grains show characteristic zoning patterns in Ti, Fe, and Cr, as has been documented in previous studies (Mevel & Kienast, 1980; Ueno, 1999; Vitale Brovarone et al., 2014; Fornash et al., 2019; Whitney et al., 2020). The types of zoning patterns mostly differ by element and vary from sample to sample. Fe is commonly concentrically zoned (Fig. 8a); some grains have an Fe-richer rim and others have an Fe-richer core. Some grains exhibit irregular zoning patterns in Fe (Fig. 8b; Table 3); in particular, grains that have been partially replaced by other phases, such as calcite (i.e. Rio San Juan blueschist-facies metagabbro IEC15-3.5). In the Tavşanlı metasomatite (TZ10-2.2C), Fe zoning is patchy in the core, and between the core and rim regions there are domains of higher or lower Fe (Fig. 8c).

Ti in lawsonite typically displays either concentric or hourglass sector zoning (Table 3). Ti-hourglass zoning is characterized by a locally preserved Ti-intermediate core (Zone 1), Ti-rich mantle (Zone 2), and Ti-poor rim (Zone 3) (Fig. 8d and e); we adopt here the zone definitions used by Vitale Brovarone et al. (2014) for lawsonite in Corsica metasomatites. An additional outermost rim domain (Zone 4) with variable Ti-content and prominent Cr-oscillatory zoning (Fig. 8e) was recognized in lawsonite from the Sivrihisar blueschist (SV01-75A), which has the

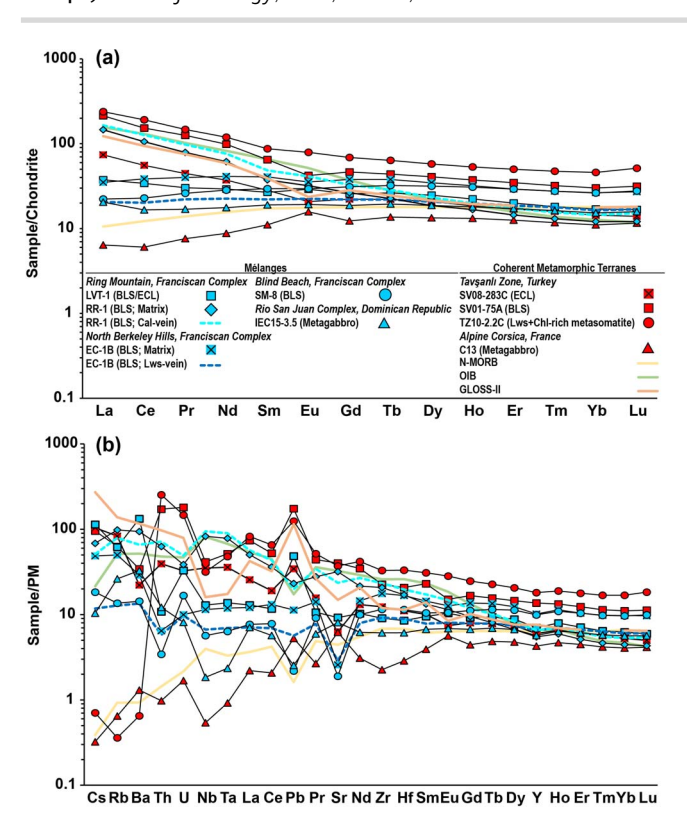


Fig. 6. REE and TE abundances of lawsonite-bearing metabasites, metasomatite, and veins. (a) Chondrite-normalized REE patterns. (b) PM-normalized TE patterns. Normalization values are from Palme & O'Neill (2007) (PM), Sun & McDonough (1989) (Chondrite, N-MORB, OIB), and Plank (2014) (GLOSS-II).

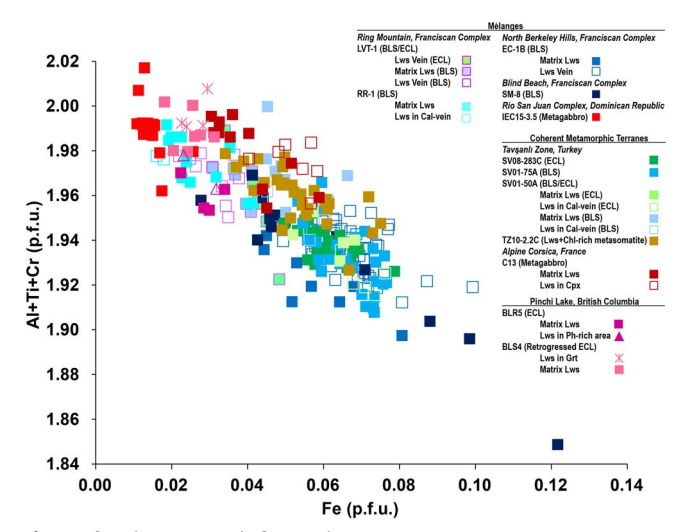


Fig. 7. Al + Ti + Cr vs. Fe in lawsonite.

highest Cr concentration (up to 1 wt% Cr₂O₃). Ti zoning in some grains correlates with the same type of zoning in Fe; e.g. in the Franciscan (Ring Mt) blueschist RR-1, matrix lawsonite locally shows Fe-oscillatory zoning that negatively correlates with Ti-oscillatory zoning (Fig. 8f).

Cr zoning is rare in the lawsonite analyzed, but where present, it generally follows Fe zoning (Table 3). A few exceptions include matrix lawsonite in the Sivrihisar blueschist (SV01-75A) (Fig. 8e). The Pinchi Lake grains

in the phengite-rich region (BLR4) display Fe-oscillatory zoning, with Cr-rich domains in the core (Fig. 8g).

REE compositions

REE in lawsonite vary in concentrations and patterns at both sample and grain scales. In general, matrix lawsonite from metabasite samples displays LREE enrichments relative to middle REE (MREE) and/or heavy REE (HREE) (La/Dy_N = 1-24.7, La/Yb_N = 1.03-97.3) with a slight-to-significant negative Eu anomaly (Fig. 9a and b; Table 3). Matrix lawsonite from the Rio San Juan blueschist-facies metagabbro (IEC15-3.5), one Franciscan blueschist (Ring Mt RR-1), and the Corsica Lws-Omp metagabbro (C13) show a positive Eu anomaly (Fig. 9a and b).

In the Pinchi Lake retrogressed eclogite (BLR4), lawsonite in garnet is lower in REE $(1 \times - \sim 10 \times \text{ chondrite})$ than matrix lawsonite ($\sim 1 \times - \sim 1000 \times$ chondrite) and it displays a positive REE pattern (La/Yb_N = 1.89-5.57) with a positive Eu anomaly (Fig. 9c). Matrix lawsonite is generally enriched in LREE relative to M-HREE (La/Yb_N = 1.45-856) with no Eu anomaly (Fig. 9c; Table 3). Lawsonite in garnet and in the matrix from the Pinchi Lake eclogite (BLR5) mostly show nearly flat REE patterns with a few matrix grains displaying positive-sloped patterns $(La/Yb_N = 1.29-129)$ (Fig. 9d). Lawsonite in phengite-rich areas of eclogite BLR5 exhibits a positive-sloped REE pattern (La/Yb_N = 15.1–116) and has higher REE contents $(\sim 1 \times - \sim 1000 \times \text{ chondrite})$ than matrix lawsonite and lawsonite inclusions in garnet (\sim 1 × $- \sim$ 100× chondrite) (Fig. 9d).

Lawsonite in the Tavşanlı metasomatite (TZ10-2.2C) contains higher REE concentrations than lawsonite in Sivrihisar metabasites (SV01-75A, SV08-283C) $(\sim 1 \times -\sim 1000 \times \text{ chondrite vs. } 1 \times -\sim 100 \times \text{ chondrite})$ with great variations in REE patterns (La/Yb_N = 0.09-1.95) (Fig. 9b and e) and a slight negative-to-positive Eu anomaly (Fig. 9e). In the Sivrihisar blueschist/eclogite (SV01-50A), no significant differences were observed in REE patterns and concentrations between lawsonite in the matrix and in the calcite-vein (Fig. 9b and e). In contrast, vein-lawsonite in two Franciscan blueschists (N Berkeley Hills EC-1B, Ring Mt RR-1) differs in REE patterns and concentrations from matrix lawsonite in the same samples; vein-lawsonite mostly shows a negative-sloped REE pattern (La/Yb_N = 0.11-0.94) with lower LREE concentrations ($\sim 1 \times - \sim 100 \times$ chondrite vs. \sim 1 × $-\sim$ 1000× chondrite) (Fig. 9a and f). In the Corsica Lws-Omp metagabbro (C13), lawsonite that occurs in the partially replaced areas of omphacite exhibits great variations in REE patterns (La/Yb_N = 0.08-0.41) with higher REE concentrations ($\sim 1 \times -100 \times$ chondrite vs. $\sim 1 \times - \sim 10 \times$ chondrite) compared with matrix lawsonite (Fig. 9b). Vein-lawsonite consisting of lawsonite-rich layers (veins) in Ring Mt blueschist/eclogite (LVT-1) has L-MREE concentrations higher than matrix lawsonite in the blueschist layers of LVT-1 (\sim 1 × -100× chondrite vs.

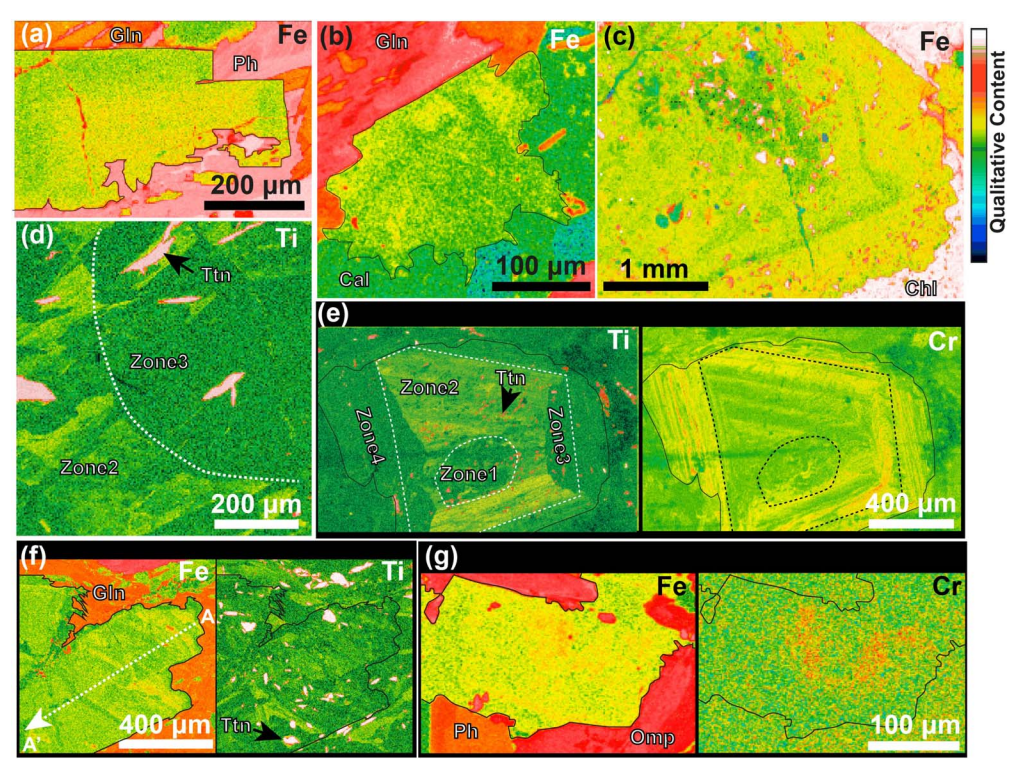


Fig. 8. Fe, Ti, and Cr zoning patterns in lawsonite. (a) Fe concentric zoning in matrix lawsonite (Ring Mountain blueschist/eclogite LVT-1). (b) Irregular Fe zoning in matrix lawsonite, partially replaced by calcite (Rio San Juan metagabbro IEC15-3.5). (c) Irregular Fe zoning in matrix lawsonite with oscillatory pattern toward the rims (Tavsanlı metasomatite TZ10-2.2C). (d) Ti hourglass zoning in lawsonite-vein with Ti-rich (Zone 2) and Ti-poor (Zone 3) domains (Ring Mountain blueschist/eclogite LVT-1). White dotted line indicates the boundary between different zones. (e) Ti and Cr zoning in one lawsonite crystal in the matrix (Sivrihisar blueschist SV01-75A). Ti-hourglass zoning shows four distinct domains, including Ti-intermediate (Zone 1), Ti-rich (Zone 2) and Ti-poor (Zone 3) domains. Zone 4 is the outermost domain with prominent Cr-oscillatory zoning and a range of Ti content. White and black dotted lines indicate the boundaries between different zones. (f) Fe and Ti oscillatory zoning in one lawsonite crystal in the matrix (Ring Mountain blueschist RR-1). (g) Fe and Cr zoning in one lawsonite crystal in a phengite-rich area (Pinchi Lake eclogite BLR5). Black solid lines: grain boundaries of lawsonite grains.

 $1 \times -\sim 10 \times$ chondrite; Fig. 9a and f) and it shows variable REE patterns; vein-lawsonite in garnet blueschist layers show LREE enrichments (La/Yb_N = 0.31-2.37), whereas that in eclogite layers show HREE enrichments $(La/Yb_N = 0.06-0.65)$ (Fig. 9f; Table 3).

Other TE compositions

Pb, Sr, V, and Cr are present at trace levels in most analyzed lawsonite grains (Tables 3 and 4; Supplementary Table S1), with concentrations varying at the intragrain and intergrain scales. A compilation of published data and our analyses suggests that Pb and Sr contents in lawsonite are positively correlated, with distinct trends in Sr/Pb (Martin et al., 2014; Fornash et al., 2019; Whitney et al., 2020); lawsonite in quartz-rich metasediment tends to have lower Sr/Pb than lawsonite in metabasite (4-25 vs. >30; Fig. 10a). Lawsonite in calcschist generally has Sr/Pb within the range of lawsonite in metabasite (>30; Supplementary Table S1).

Most analyzed matrix grains have Sr/Pb comparable with lawsonite from metabasalt with moderate Sr/Pb (30-50; Fig. 10a), with a few exceptions: the Pinchi Lake eclogites (BLR4, 5) and Sivrihisar blueschist/eclogite (SV01-50A). In the Pinchi Lake retrogressed eclogite (BLR4), some matrix grains have lower Sr/Pb in the region

between core and rim than in the core/rim regions (16-18 vs. 30-181; Table 3). In contrast, matrix grains in the Sivrihisar blueschist/eclogite (SV01-50A) have lower Sr/Pb in the core than in the mantle/rim regions (17–20 vs. 29–71; Table 3). These low Sr/Pb ratios are comparable with those of lawsonite from quartz-rich metasediment (4-25; Whitney et al., 2020).

Intergrain-scale variations were observed in the Rio San Juan blueschist-facies metagabbro (IEC15-3.5); matrix grains replaced by calcite have a lower range of Sr/Pb than those with no replacement (184-542 vs. 185-1083; Fig. 10b and c). Notwithstanding the different field settings of the host subduction complex, matrix grains from metagabbro (Corsica C13, Rio San Juan IEC15-3.5) have a higher range of Sr/Pb than those from metabasalt (129-1775 vs. 16-453; Fig. 10b and c). The extent of Sr/Pb variations is significantly high in lawsonite from metagabbro as compared with lawsonite from metabasalt (Fig. 10b and c).

Lawsonite in veins and in domains such as the partially replaced areas of omphacite in Corsica C13 and the phengite-rich area in the Pinchi Lake eclogite BLR5 mostly show a positive correlation between Pb and Sr (Fig. 10d). These grains have a range of Sr/Pb that differs from matrix grains and/or garnet inclusions in the

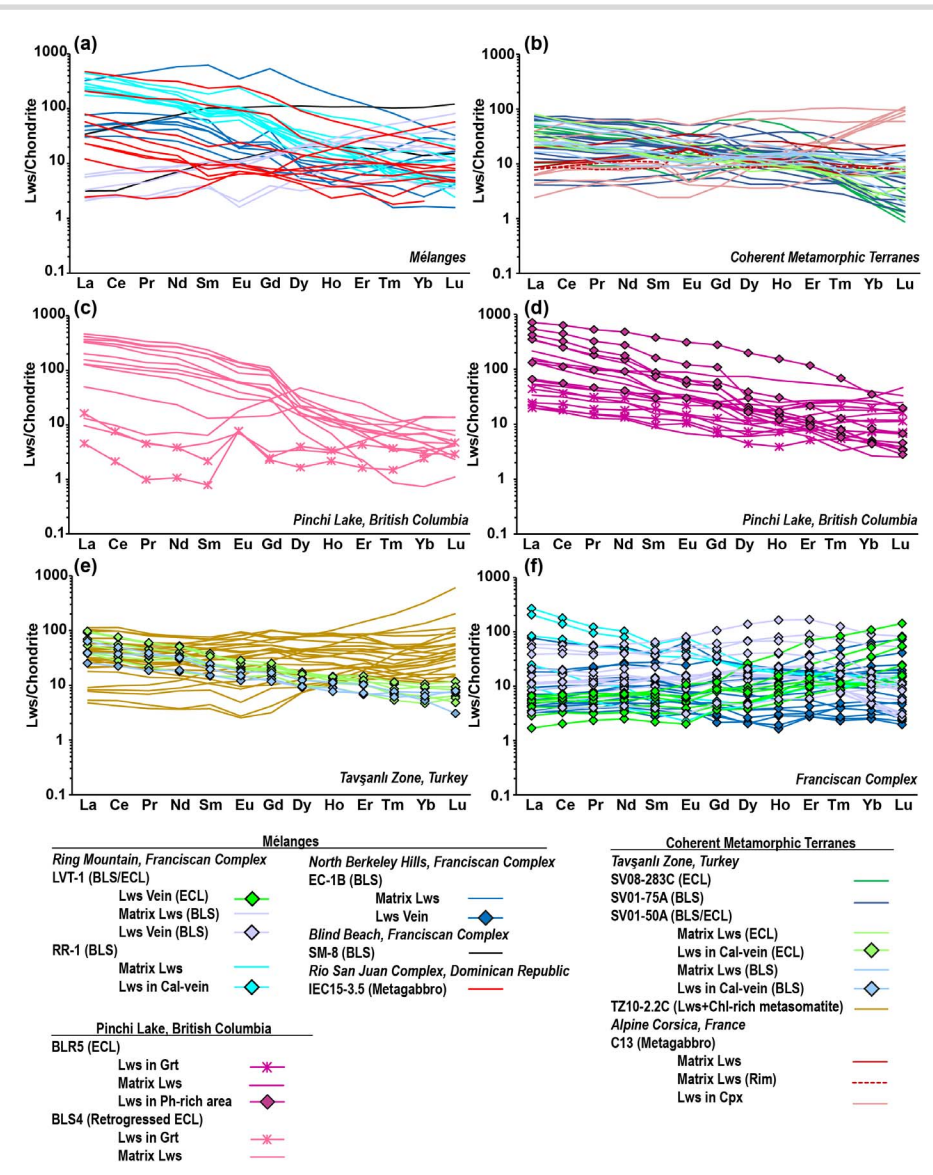


Fig. 9. REE patterns of lawsonite. (a, b) Matrix lawsonite in metabasite from mélange (a) and coherent-metamorphic terranes (b). (c, d) Lawsonite in Pinchi Lake retrogressed eclogite (c) and eclogite (d). (e) Lawsonite in the matrix from Tavşanlı metasomatite and in the vein from Sivrihisar metabasalt. (f) Lawsonite in the vein from Franciscan metabasalts.

same samples. Matrix lawsonite in the Ring Mt blueschist (RR-1) has a higher range of Sr/Pb than lawsonite in the calcite-rich vein (Fig. 10b-d; Table 3). In the Pinchi Lake eclogites (BLR4, 5), lawsonite in garnet has Sr/Pb similar to or higher than matrix lawsonite, whereas lawsonite in the phengite-rich areas of the eclogite (BLR5) has Sr/Pb similar to matrix lawsonite (Fig. 10b-d).

V concentration in lawsonite ranges from ~39–2866 ppm (Table 3; Supplementary Table S1). In general, lawsonite in quartz-rich metasediment has a similar range of V but a lower range of Cr compared with lawsonite in calcschist and metabasite (Supplementary Table S1). The V and Cr abundances of most matrix grains are positively correlated (Fig. 10e), but in some cases display intragrain variations (Fig. 10b, c and e). Matrix lawsonite from the Sivrihisar blueschist (SV01-75A) shows the most significant variations in Cr/V, with Cr/V values increasing from Zone 1 to Zone 4

(Fig. 10b; Table 3). In contrast to matrix grains, some vein-associated lawsonite exhibit no obvious correlation between Cr and V (Fig. 10f). Vein-lawsonite in Franciscan metabasalts (EC-1B, LVT-1) has higher Cr/V than matrix lawsonite (Fig. 10b and c; Table 3).

Garnet composition

Matrix garnets in the Sivrihisar blueschist and eclogite (SV01-75, SV08-283C) and the Pinchi Lake eclogites (BLR4, 5) were analyzed. Matrix garnet in the Sivrihisar blueschist (SV01-75A) and eclogite (SV08-283C) is Feand Ca-rich, and it is compositionally zoned with the core depleted in Fe and enriched in Mn relative to the rim; core: alm₅₀₋₅₈sps₆₋₁₆prp₄₋₁₀grs₂₅₋₃₀; rim: alm₅₅₋₆₂sps₄₋₈prp₇₋₁₀grs₂₄₋₃₁ (Fig. 11a). An oscillatory zoned outer-rim is locally preserved on garnet from the Sivrihisar eclogite, with higher Mn correlated with lower Fe; Mn-rich region: alm₅₁₋₅₂sps₁₄₋₁₅prp₆grs₂₇₋₂₈;

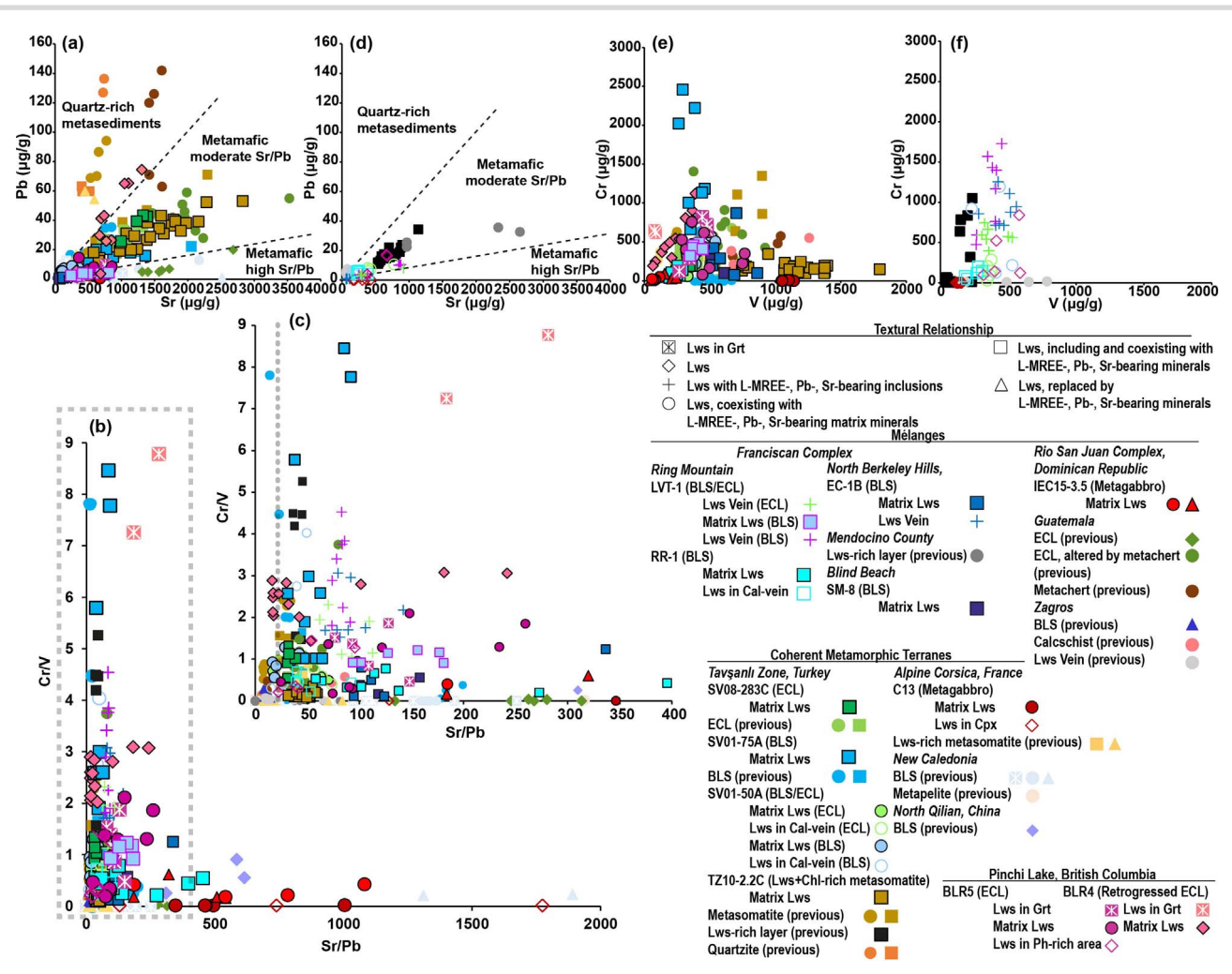


Fig. 10. (a) Pb vs. Sr in lawsonite in garnet and matrix (modified from Whitney et al., 2020). (b, c) Plots of Cr/V vs. Sr/Pb in lawsonite. Inset of Fig. 10(c) is a magnified image, showing a selected area of the original plot (marked with dashed lines). Gray dotted line delineates the range of Sr/Pb in lawsonite from quartz-rich metasediment (<25) vs. lawsonite from metabasite (>25). (d) Pb vs. Sr in lawsonite that occurs in texturally distinct domains (e.g. veins, partially dissolved areas of omphacite, phengite-rich area). (e, f) Cr vs. V in lawsonite that occurs in various textural sites (e: matrix, garnet; f: texturally distinct domains). Also shown are previous analyses of lawsonite from Franciscan Complex (Martin et al., 2014), South Motagua Mélange Zone/Guatemala (Hara et al., 2018), Sivrihisar Massif/Turkey (Fornash et al., 2019; Fornash & Whitney, 2020), Alpine Corsica/France (Martin et al., 2014; Vitale Brovarone et al., 2014), Western Alps/France (Lefeuvre et al., 2020), New Caledonia (Spandler et al., 2003), North Qilian/China (Xiao et al., 2013), and Zagros Orogen/Iran (Muñoz-Montecinos et al., 2021).

Mn-poor region: alm₅₇₋₅₉sps₇prp₇grs₂₇₋₂₈ (Fig. 11a). In the Sivrihisar blueschist, matrix garnet is locally surrounded by a Mn-rich outer-rim with the composition of alm₅₀₋₅₄sps₁₂₋₁₉prp₄grs₂₇₋₃₀. From core to oscillatory zoned outer-rim, matrix garnet in the eclogite shows noticeable increases in REE abundances ($\sim 1 \times - \sim 100 \times$ vs. $\sim 1 \times - \sim 1000 \times$ chondrite; Fig. 11b). This contrasts to the Mn-rich outer-rim on matrix garnet in the blueschist, which has M-HREE abundances similar to core-to-rim $(\sim 1 \times - \sim 100 \times \text{ chondrite}; \text{ Fig. 11b})$. Matrix garnet in both eclogite and blueschist is characterized by a negativesloped pattern (Dy/Yb_N = 0.02-0.37).

Matrix garnet in the Pinchi Lake eclogites (BLR4, 5) displays a gradual decrease in Mn, but increases in Fe and Mg from core to rim (Fig. 11a); core: alm₄₄₋₆₈sps₂₋₃₃prp₃₋₁₀ grs_{20-23} ; rim: $alm_{64-68}sps_{1-5}prp_{9-12}grs_{20-23}$. This garnet is characterized by the enrichment of MREE relative to LREE and HREE (La/Dy_N = \leq 0.02; Dy/Yb_N = 1.60-4.91), with lower M-HREE concentrations in the rim than the core $(\sim 10 \times - \sim 100 \text{ vs.} \sim 10 \times - \sim 1000 \times \text{ chondrite}; \text{ Fig. 11c}).$

Apatite composition

The REE composition of one apatite grain in the matrix of the N Berkeley Hills blueschist (EC-1B) was analyzed. This matrix grain has a negative-sloped REE pattern (La/Yb_N \leq 0.02) and its REE contents increase from core to rim (Fig. 11d).

DISCUSSION

Lawsonite composition can vary in response to (1) the compositional evolution of the host rock, (2) changes in relative mineral abundances, (3) element-fractionation with minerals, and/or (4) element selectivity that differs for each growth plane of lawsonite. We evaluate the influence of each factor on lawsonite composition

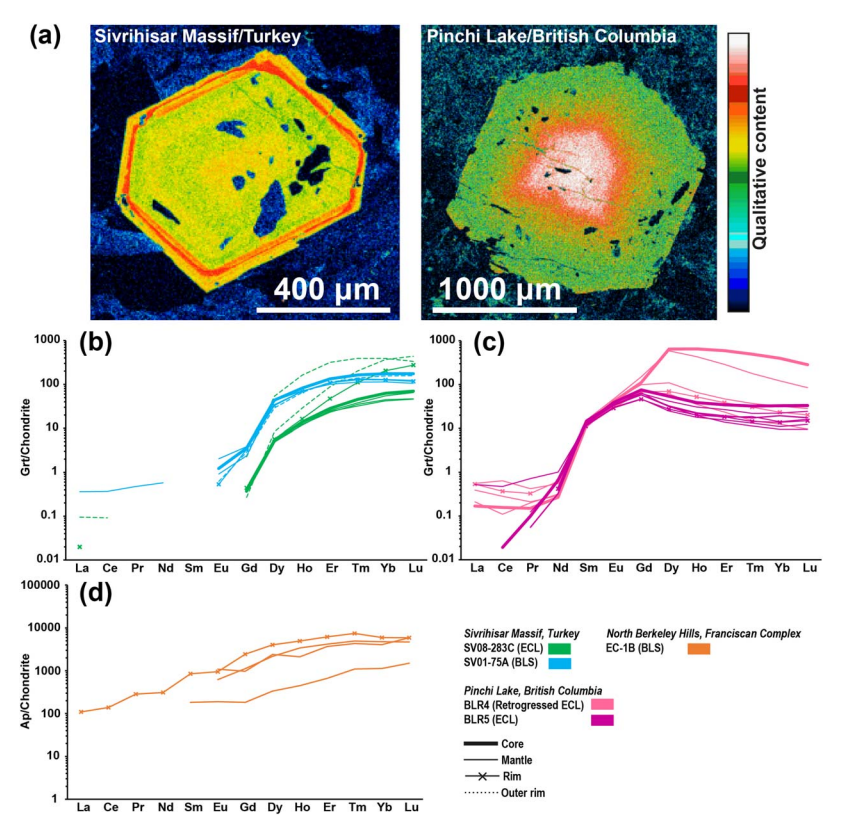


Fig. 11. (a) Mn zoning patterns in matrix garnet from Sivrihisar eclogite (SV08-283C) and Pinchi Lake eclogite (BLR5). (b, c) REE patterns of matrix garnet in Sivrihisar metabasalts (SV08-283C, SV01-75A) (b) and Pinchi Lake eclogites (BLR4, 5) (c). (d) REE patterns of matrix apatite in North Berkeley Hills blueschist (EC-1B).

to investigate metamorphic reaction history, fluid-rock interactions, and the potential sources of fluids in subduction systems.

Compositional evolution of lawsonite-bearing host rocks

The lawsonite-bearing samples have a range of bulk-rock compositions (e.g. metabasite, metasomatite; Table 2), which may have deviated from their protolith compositions owing to seafloor alteration, metamorphic reactions, metasomatism, and/or mechanical mixing. Any changes in host rock compositions during lawsonite growth likely induced compositional variations in lawsonite. To evaluate the controls of host rock signatures on lawsonite composition, it is critical to understand the compositional evolution of host rocks.

Based on a V vs. Ti/1000 diagram, most metabasalt samples from Franciscan mélange areas and the Sivrihisar coherent terrane plot in the MORB/back-arc basin basalt (BABB) field (Fig. 12a), except a Ring Mt blueschist (RR-1) that has an oceanic island basalt (OIB) signature (Fig. 12a). This is partially inconsistent with the results of an Hf-Th-Ta diagram, in which the Sivrihisar eclogite (SV08-283C) and blueschist (SV01-75A) are classified as having a calc-alkaline basalt (CAB) and a within-plate basalt signature, respectively (Fig. 12b). This inconsistency is not surprising given the high bulk Th contents of the Sivrihisar metabasalts (Table 2), which result in high Th/La, causing the Sivrihisar metabasalts

plot outside the MORB field in a Th/La vs. Sm/La diagram (Fig. 12c). Th/La has been interpreted to be less fractionated during subduction and its high value (i.e. >0.35 in terrigenous sediment) is likely derived from interactions with (meta)sediment (Plank, 2005) and/or (meta)sediment-sourced fluids before or during subduction metamorphism (Fig. 12c). The high K₂O content and the LREE and LILE enrichments of the Sivrihisar metabasalts further support the possible influence of (meta)sediment (Figs 5 and 6). This interpretation is consistent with high Nb/Cr ratio in matrix rutile observed in Sivrihisar metabasalt, which is comparable with rutile in metapelite (Fornash & Whitney, 2020). In the case of Sivrihisar blueschist (SV01-75A), Cr and Ni enrichments (Fig. 5) indicate the additional influence of ultramafic rocks (e.g. serpentinite, metagabbro). Serpentinite can also act as a source for LILE (e.g. Cs and Ba) (Tenthorey & Hermann, 2004; Deschamps et al., 2011, 2013).

The Franciscan metabasalts, classified as MORB/BABB, are enriched in LILE and LREE, with higher K₂O content relative to N-MORB (Figs 5 and 6). This suggests some extent of interaction with (meta)sediment or (meta)sediment-sourced fluid, possibly via mechanical mixing, which is common in mélange. Alternative LILE sources include serpentinite (Scambelluri et al., 2001, 2004; Tenthorey & Hermann, 2004), altered basaltic crust (Ryan et al., 1995; Becker et al., 2000; John et al., 2008), and/or fluids sourced from these lithologies. The high Cr and Ni contents of the Ring Mt blueschist/eclogite

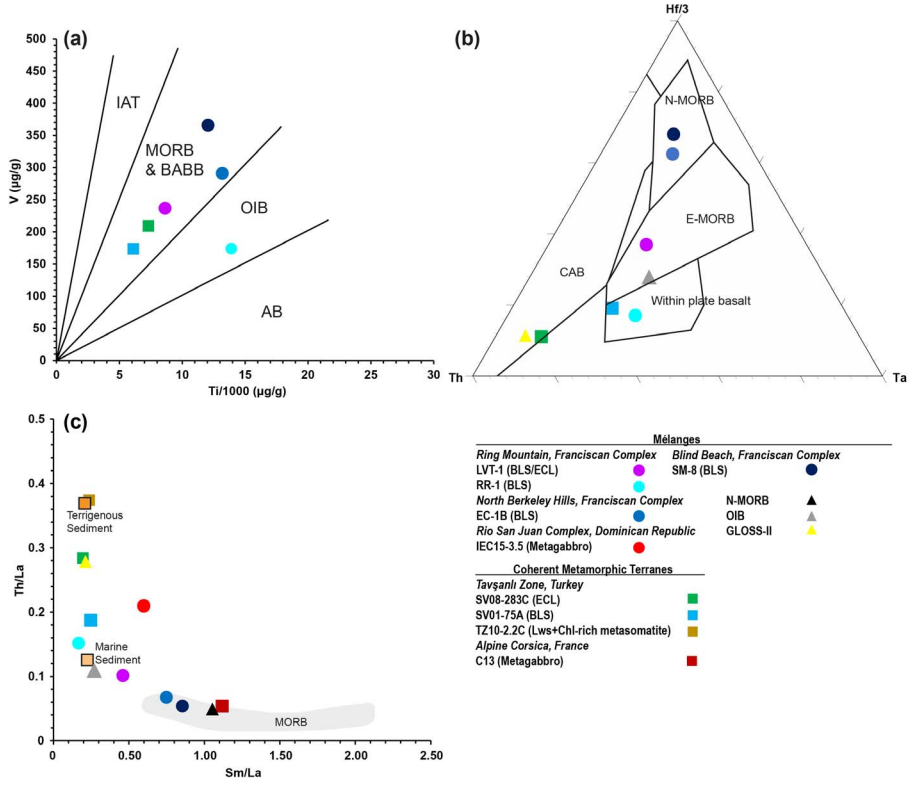


Fig. 12. Discrimination diagrams for metabasite and metasomatite. (a) V vs. Ti/1000 (Shervais, 1982). (b) Hf/3 vs. Th vs. Ta (Wood, 1980). (c) Th/La vs. Sm/La (Plank, 2005, 2014). Abbreviations: N-MORB, normal mid-ocean ridge basalt; E-MORB, enriched mid-ocean ridge basalt; BABB, back-arc basin basalt; IAT, island arc tholeiite; OIB, oceanic island basalt; AB, alkali basalt; CAB, calc-alkaline basalt.

(LVT-1) indicate additional interactions with ultramafic rocks (Fig. 5). The LILE and LREE enrichments of the Ring Mt blueschist (RR-1) could have been inherited from the composition of an OIB protolith (Figs 6 and 12a,b).

The Taysanlı metasomatite (TZ10-2.2C) records high Th/La—comparable with the ratio of terrigenous sediment (Fig. 12c)—but it shows significant K₂O and LILE depletions (Figs 5 and 6b). The high MgO and significantly low SiO₂ of this metasomatite indicate an ultramafic protolith (Fig. 5; Table 2), consistent with low K₂O and LILE abundances. The high Th/La and the LREE enrichment, however, suggest interactions with terrigenous sediment during metasomatism.

The Corsica Lws-Omp metagabbro (C13) has no clear compositional indication of alteration by (meta) sediment, whereas the Rio San Juan blueschist-facies metagabbro (IEC15-3.5) preserves evidence for interactions with (meta)sediment (e.g. high Th/La, bulk enrichments in LILE and LREE relative to N-MORB; Figs 6 and 12c). Except for the Corsica metagabbro, all samples preserve compositional signatures supporting interactions with (meta)sediment \pm metagabbro/serpentinite, although it is unclear when and how the samples obtained these signatures.

Bulk-rock-normalized element concentrations and element budget of lawsonite

Lawsonite composition can be closely related to the host rock composition, but this may be simultaneously influenced by other factors (e.g. changes in mineral modes). To interpret controls of host rock signatures on lawsonite composition, the TE composition of matrix lawsonite was averaged and normalized to the corresponding bulk composition of its host rock (Fig. 13a). If lawsonite composition was continuously equilibrated with evolving host rock composition, lawsonite would have inherited its elemental signatures entirely from the host rock. In this case, the value of normalization would be close to unity. In contrast, any deviation from unity would be expected with the increasing influence of factors other than the host rock signature. The normalized TE concentrations (referred to as 'Bulk' in the subscript of element concentrations) were then compared with the TE budgets of matrix lawsonite.

In most cases, the average element concentrations of matrix lawsonite are lower than the corresponding bulk concentrations of the host matrix (<1 in Fig. 13a), and matrix lawsonite hosts less than 100% of bulk REE and TEs (Fig. 13b and c). Such matrix grains host variable proportions of bulk Sr, Pb, REE, Th, U, Cr, and V (up to 100%), and low proportions (<30%) of bulk LILE (i.e. Rb, Ba) and high field strength elements (HFSE; Zr, Hf) (Fig. 13b and c). The calculated element budget is consistent with the previous mass balance calculations of lawsonite-bearing HP/LT rocks (Spandler et al., 2003; Martin et al., 2014; Hara et al., 2018; Whitney et al., 2020). LILE- (e.g. phengite, glaucophane), L-MREE- (e.g. apatite, titanite, epidote), and U/Th-bearing phases (e.g. apatite,

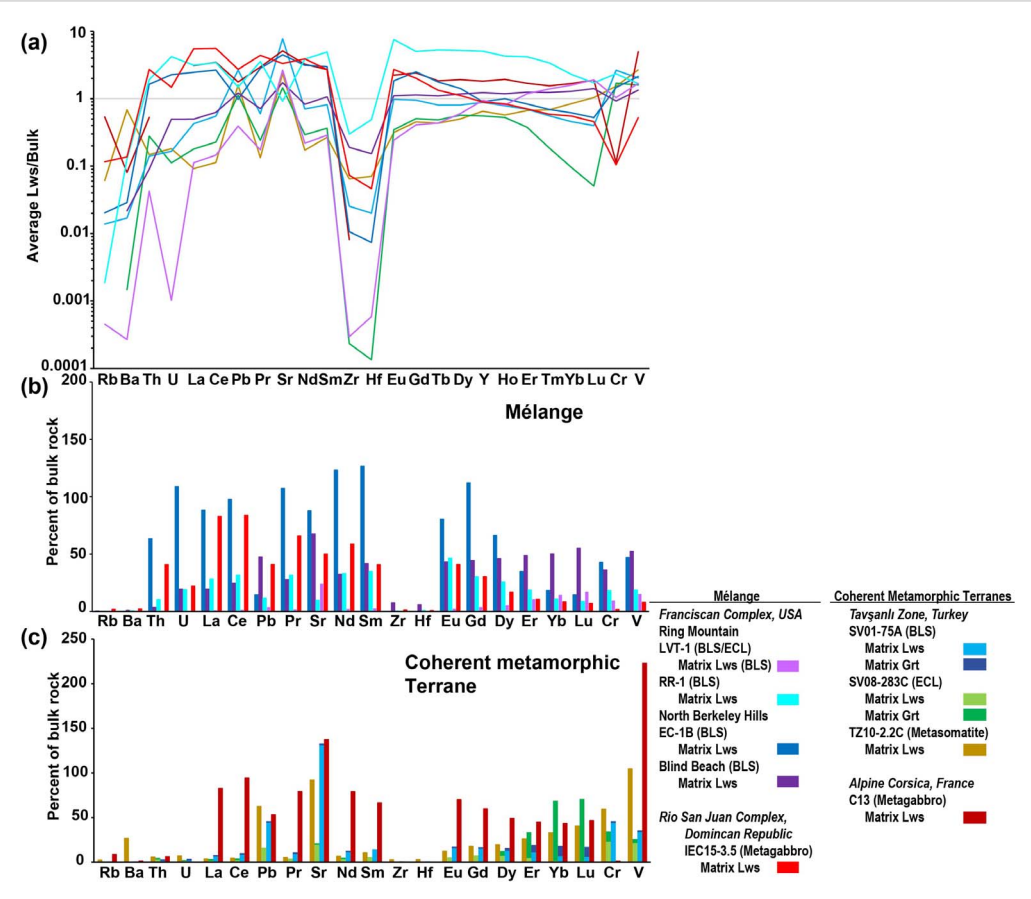


Fig. 13. (a) Bulk-rock-normalized average element concentrations of matrix lawsonite. (b, c) Element budgets of matrix lawsonite and matrix garnet.

titanite) occur in the matrix of most samples analyzed (Table 1). Therefore, the concurrent growth of these minerals can explain the low abundances of these elements in lawsonite.

In contrast, some matrix lawsonite grains apparently host more than 100% of bulk REE and TEs (e.g. Sr, V) and the average concentrations of these elements are higher than the bulk-rock concentrations (>1) (e.g. Sivrihisar blueschist SV01-75A; Fig. 13). Such overestimated element budgets have also been reported (Spandler et al., 2003; Martin et al., 2014) and interpreted as the influence of μ m-sized inclusions in lawsonite. Possible Sr-, Vand/or REE-bearing inclusions in lawsonite are epidote, apatite, and titanite (Table 1).

In contrast, matrix lawsonite in the Rio San Juan blueschist-facies metagabbro (IEC15-3.5) and the Ring Mt blueschist (RR-1) accounts for less than 90% of bulk L-MREE and 40% of bulk Th and U, although the average concentrations of these elements are higher than bulk-rock concentrations (Fig. 13a and b). This can be explained by (1) the absence or low modal abundance of minerals that compete for these elements and/or (2) low lawsonite mode. Lawsonite in IEC15-3.5 best exemplifies the former case, given the absence of U, Th, L-MREE-bearing competitors except for minor epidote (Table 1) and texturally late calcite (Fig. 3j). However, lawsonite in RR-1 occurs as a major matrix

phase and coexists with other U, Th, L-MREE-bearing minerals (e.g. titanite, apatite; Table 1). This requires alternative explanations, such as the following: (1) lawsonite mode was underestimated; (2) some domains of matrix lawsonite equilibrated with a bulk-rock composition that was richer in L-MREE, U, and Th than the measured bulk composition; and/or (3) the measured lawsonite composition may not represent the average composition.

Matrix garnet from the Sivrihisar blueschist (SV01-75A) and eclogite (SV08-283C) is a major host mineral of HREE (Fig. 11b), explaining the HREE depletion of coexisting lawsonite (Fig. 13c). Although the bulk-rocknormalized average element concentrations and element budget of matrix lawsonite are useful to assess the influence of factors other than host rock signatures (e.g. element fractionation by coexisting minerals), they might de-emphasize the records of zoning by averaging the compositional variations of individual minerals. Therefore, the following sections investigate the zoning records of individual lawsonite grains.

Compositional variations in lawsonite

The possible mechanism of Ti, Fe, and Cr zoning in lawsonite is discussed in relation to variations in other TEs (e.g. REE, Pb, Sr).

Crystallographic control of Ti/REE in lawsonite: hourglass sector zoning

Sector zoning may reflect coeval differences in element selectivity on different growth planes in response to reaction overstepping and fast growth rate (Watson & Liang, 1995; Stowell et al., 2011). Such differences can be retained in the crystal as a result of slow intracrystalline diffusion rates (Wass, 1973; Watson & Liang, 1995). Tihourglass sector zoning was observed in lawsonite from blueschist and vein in the Ring Mt blueschist/eclogite (LVT-1), from the Sivrihisar blueschist (SV01-75A), and from the partially replaced area of omphacite in Corsica Lws-Omp metagabbro (C13).

In all these samples, Ti-rich Zone 2 displays REE patterns similar to Zone 1, but has noticeably lower REE contents than Zone 1 (Fig. 14a-d), possibly as a result of the rapid growth of Zones 1 and 2 (Wass, 1973; Ueno, 1999; Vitale Brovarone et al., 2014). In general, Ti-poor Zone 3 has similar to slightly different REE patterns as compared with the associated Zones 1 and 2, and the overall REE abundances are higher than Zone 2 (Fig. 14a, b, e and f). Zone 3 might have readily incorporated REE relative to the other Zones as suggested by Ueno (1999), who documented REE enrichments in the {100} sector, which grows along [100] and [ī00] based on his nomenclature. However, Zone 3 in Corsica lawsonite (C13) shows a selective enrichment in HREE relative to the associated Zone 2 (Fig. 14c). Metasomatic lawsonite documented in the previous study of Corsica metasomatite is characterized by continuously decreasing REE contents and a consistent REE pattern across Zones 1–3, possibly owing to the fast growth of Zones 1–3 (Vitale Brovarone et al., 2014). From this perspective, Zone 3 in lawsonite can have variable REE abundances with a similar to significantly different REE pattern compared with the associated Zones 1 and 2. This suggests that factors other than crystallographic control (e.g. element fractionation between minerals, fluid-rock interactions, fast crystal growth) simultaneously influenced REE partitioning in Zone 3. For instance, the selective HREE enrichment in Zone 3 of Corsica lawsonite may either signal the infiltration of HREE-rich fluids or L-MREE fractionation with coexisting minerals (Fig. 14c). In the case of Sivrihisar lawsonite, Zone 4 shows significant variations in HREE contents compared with Zone 1-3 (Fig. 14g), possibly indicating the intermittent influence of HREE-rich fluids and/or interactions with HREE-rich garnet (Fig. 11b).

All domains, including Zone 4, have TE patterns characterized by strong depletions in HFSE and LILE (Fig. 14b, d, and f). Pb and Sr anomalies are variable within the zones (Supplementary Table S1), but their variations among the zones are largely controlled by the abundance of LREE that have a similar compatibility with Pb and Sr (e.g. Ce, Pr). Pb and Sr anomalies tend to be higher in REE-poor Zone 2 relative to REE-richer Zones 1 and 3 (e.g. Sivrihisar blueschist SV01-75A, vein in the blueschist layers of LVT-1; Fig. 14g) unless the changes in Sr and Pb concentrations across Zones 1-3

counterbalance the effect of variations in LREE contents (e.g. Zone 3 of vein-lawsonite with a higher Sr anomaly in the eclogite layers of LVT-1; Fig. 14g and h). In addition, U-Th fractionation $(0 \le (U/Th)_{PM} \le 54.9)$ are significantly variable within and among the zones (Fig. 14b, d, and f) mainly due to the low U and Th contents (<2 μ g/g; Supplementary Table S1). Such heterogeneous lawsonite composition corroborates the simultaneous operation of several factors (e.g. element-fractionations between minerals, fluid-rock interaction) in addition to crystallographic control. Despite the influence of other factors, our compositional analyses highlight the importance of crystallographic control on the Ti and REE contents of lawsonite.

Evidence for mineral-fluid interactions and element fractionation between minerals Fe/REE zoning

Lawsonite grains that exhibit core-to-rim zoning in Fe but not hourglass zoning in Ti in some cases show covariations between Fe and REE. Some matrix grains in the N Berkeley Hills blueschist (EC-1B) are characterized by a significant MREE depletion compared with LREE and HREE depletions at Fe-rich rims, which are illustrated as high (La/Dy)_N and low (Dy/Yb)_N (Fig. 15a and b). This indicates the concurrent growth of lawsonite with MREErich apatite (Fig. 11d) and/or titanite, both of which occur in the matrix of sample EC-1B (Table 1). In contrast, vein-lawsonite records high (Dy/Yb)_N and (La/Yb)_N at the Fe-depleted rims, reflecting an HREE depletion (Fig. 15b and c). The formation of HREE-rich pumpellyite that replaced vein-lawsonite (Fig. 3f) could explain the fractionation of Fe and HREE.

Matrix grains in the Corsica Lws-Omp metagabbro (C13) are nearly constant in (La/Dy)_N, (La/Yb)_N, and (Dv/Yb)_N regardless of Fe content (Fig. 15a-c; Table 3). Together with the constant REE patterns, Corsica matrix grains record a core-to-rim decrease in Fe and REE concentrations (Fig. 9b). This suggests REE and Fe depletions during continuous growth of lawsonite grains.

The Fe content of lawsonite in calcite-rich veins from the Ring Mt blueschist (RR-1) increases toward the rims and is positively correlated with (La/Dy)_N and (La/Yb)_N (Fig. 15a and c). One possibility to explain this relative LREE enrichment is that lawsonite in the matrix was influenced by LREE fractionation during its earlier growth, later incorporated into the vein, and subsequently influenced by LREE-rich vein-forming fluids. However, vein-associated lawsonite shows changes in REE patterns that become comparable with matrix lawsonite toward the Fe-rich rims, with REE abundances approaching the bulk concentrations of the matrix (~ 1; Fig. 15d). Therefore, vein-lawsonite might have cocrystallized with LREE-hosting aragonite during earlier growth, and gradually became equilibrated with the matrix while vein-aragonite was converted to calcite during later exhumation.

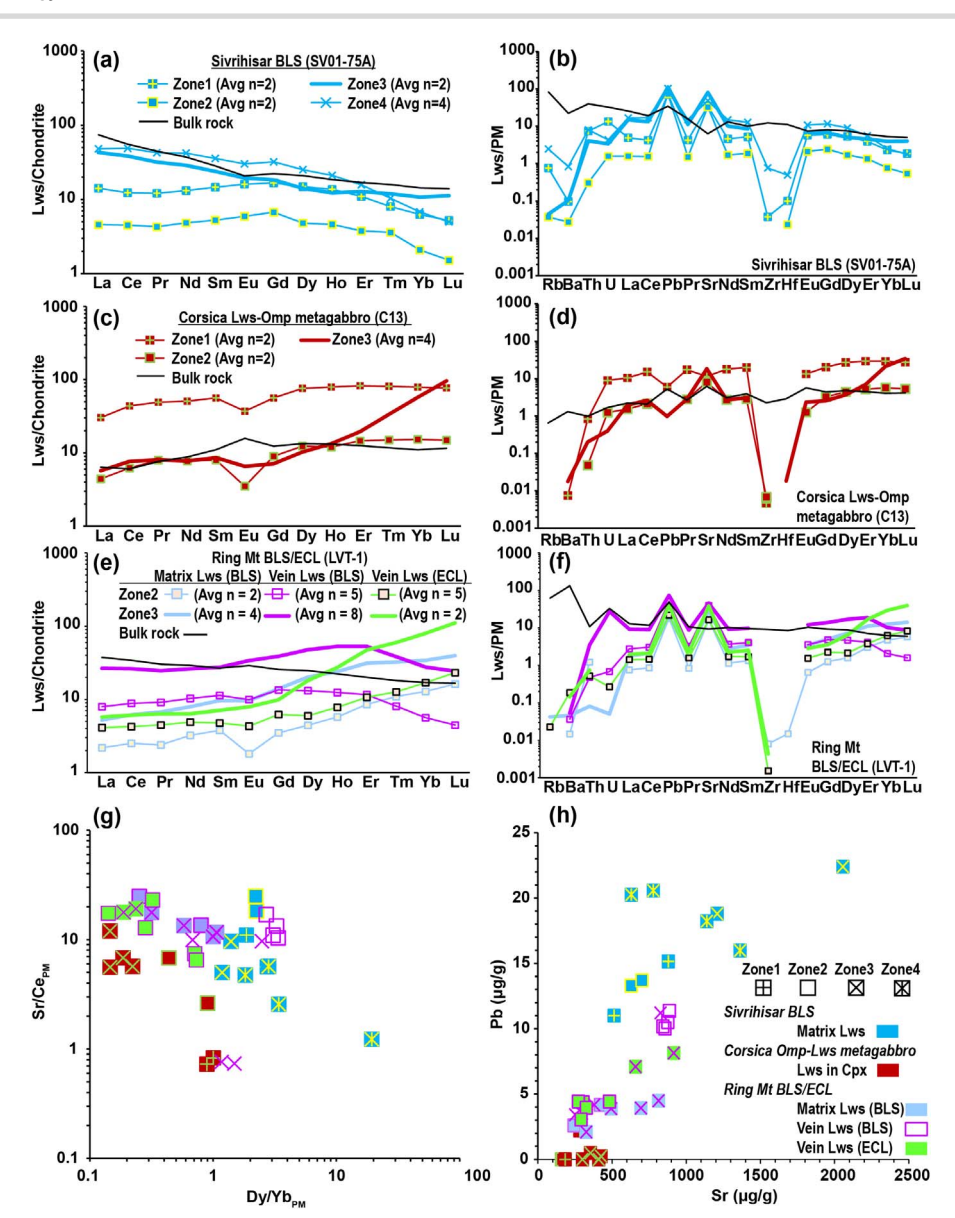


Fig. 14. (a-h) Composition of lawsonite with Ti-hourglass zoning. REE (a, c, e) and TE patterns (b, d, f) of lawsonite from Sivrihisar blueschist (SV01-75A) (a, b), Corsica Lws-Omp metagabbro (C13) (c, d), and Ring Mt blueschist/eclogite (LVT-1) (e, f). (g) (Sr/Ce)_{PM} vs. (Dy/Yb)_{PM}. (h) Pb vs. Sr.

Matrix grains in the Sivrihisar blueschist/eclogite (SV01-50A) have high $(La/Yb)_N$ and $(Dy/Yb)_N$ in the Fe-poor core (Fig. 15b and c), which corresponds to low Sr/Pb (17–20) (Fig. 10c; Table 3). This low Sr/Pb is within the range of lawsonite from quartz-bearing metasediment (Fornash et al., 2019; Whitney et al., 2020), indicating possible interactions with siliciclastic metasediment (also high in La/Yb and Dy/Yb) during the growth of core. The subsequent decreases in $(La/Yb)_N$ and $(Dy/Yb)_N$ (Fig. 15b and c) may reflect the decreasing influence of siliciclastic metasediment as suggested by a simultaneous increase in Sr/Pb (29–50; Table 3).

The $(La/Dy)_N$ of some matrix grains in the Pinchi Lake retrogressed eclogite (BLR4) initially increases and then decreases with $(La/Yb)_N$ toward the Fe-rich rims (Fig. 15a and c). The initial LREE and Fe enrichments might indicate the breakdown of LREE-hosting, Fe-rich epidote (absent in the matrix; Table 1). However, the

Pinchi Lake eclogites evolved within the stability field of lawsonite from prograde to peak conditions (Ghent et al., 1993), thereby requiring a different explanation. Interactions with siliciclastic metasediment can account for the LREE enrichment and a concomitant Sr/Pb decrease (16–18; Table 3), which falls within the range of lawsonite in quartz-rich metasediment (Fornash et al., 2019). The effect of Sr/Pb-fractionation is likely negligible given the absence of other Sr- and Pb-hosting minerals in the matrix and garnet. LREE depletion and Sr/Pb increase (32–101; Table 3) might stem from the decreasing contribution from quartz-rich (meta)sediment and/or the infiltration of LREE-depleted fluids with high Sr/Pb.

Oscillatory zoning

Lawsonite in HP/LT rocks, metasomatite, and eclogitefacies veins in some cases preserves oscillatory zoning, which has been suggested to develop as a result of

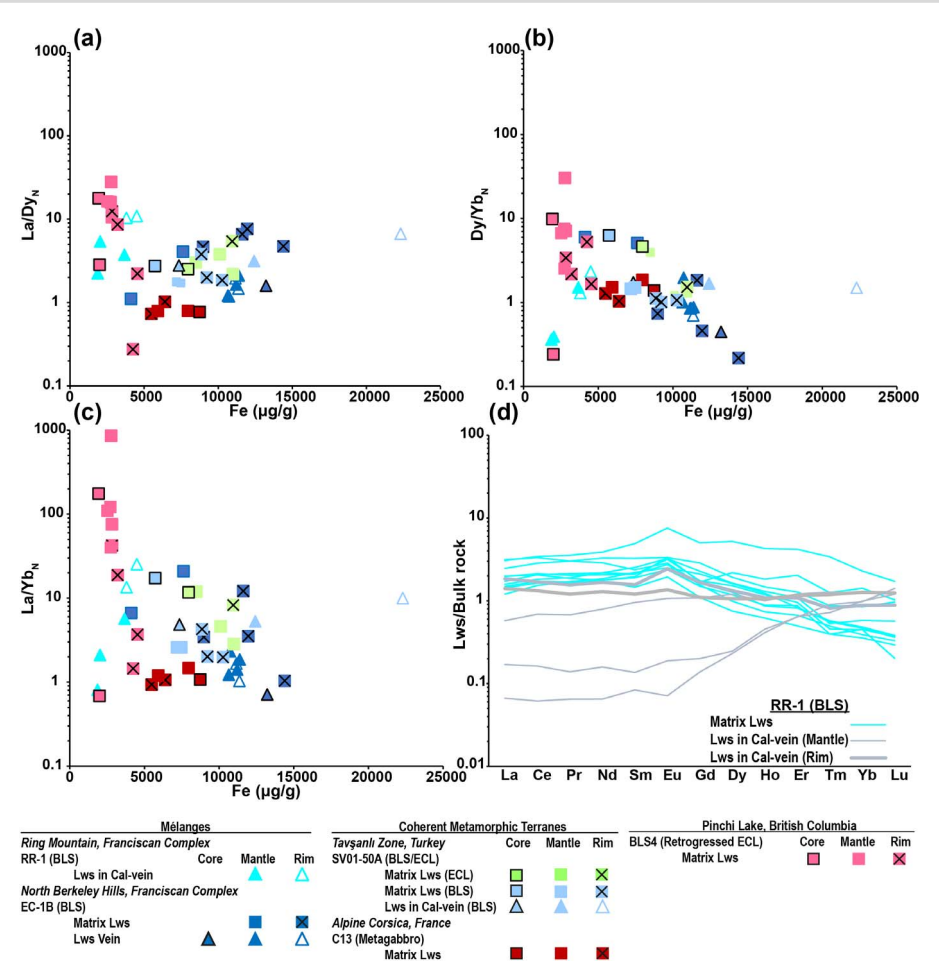


Fig. 15. (a, b, c) Lawsonite with Fe-concentric zoning, showing variations in (La/Dy)_N (a), (Dy/Yb)_N (b), and (La/Yb)_N (c). (d) Bulk-rock normalized REE patterns of lawsonite in calcite vein from Ring Mt blueschist (RR-1).

fluctuating metamorphic P-T-fO₂, and/or of intermittent element supply via fluid-infiltration or mineral breakdown reactions (Sherlock & Okay, 1999; Vitale Brovarone et al., 2014; Fornash et al., 2019; Fornash & Whitney, 2020). In the Ring Mt blueschist RR-1, matrix lawsonite locally shows Fe-oscillatory zoning that negatively correlates with Ti-oscillatory zoning (Fig. 8f). The fluctuating Fe content also covaries with (La/Dy)_N and (La/Yb)_N (Fig. 16a) owing to repeated changes in REE contents, of which M-HREE are positively correlated with Fe (Fig. 16a). Mn and Cr contents also covary with HREE content, and they show a positive and negative correlation, respectively (Fig. 16a).

One possible explanation for these element covariations is the destabilization of garnet (absent in the sample; Table 1) during the growth of lawsonite. Garnet that is oscillatory zoned in Mn occurs in zoisite-bearing interlayered eclogite/blueschist and amphibolite in the same region (Viete et al., 2018; Cruz-Uribe et al., 2021). This oscillatory pattern has been interpreted to reflect a periodic dissolution-growth cycle of garnet that developed in response to intermittent pulses of fluid flow (Viete et al., 2018; Cruz-Uribe et al., 2021). Upon the cyclic dissolution to complete breakdown of garnet, Fe, Mn and M-HREE might have been provided intermittently as lawsonite

grew along a retrograde P-T path (Fig. 2). Between the pulses of fluids, matrix lawsonite likely hosted Cr instead of Fe, Mn, and M-HREE (Fig. 16a).

Cr-oscillatory zoning was observed in matrix grains from the Sivrihisar blueschist SV01-75A, which also show Ti-hourglass zoning (Fig. 8e). In Zones 3 and 4, high Cr content coincides with high Fe and low V (Fig. 16b). A positive Cr³⁺-Fe³⁺ correlation in oscillatory zoning has been documented in Sivrihisar lawsonite and suggested to reflect the fluctuating fO2 of infiltrating fluids (Fornash et al., 2019). Given that Cr³⁺-Al³⁺ substitution in lawsonite is facilitated at oxidizing condition (Sherlock & Okay, 1999), high Cr³⁺ and Fe³⁺ and low V may indicate the relatively oxidizing condition of infiltrating fluids. Although Cr is assumed to be relatively immobile in fluids, minerals in HP metasomatic environments (e.g. eclogite-facies veins, margins of HP/LT blocks) preserve evidence supporting enhanced Cr mobility (e.g. Cr-rich domains in oscillatory zoned garnet, lawsonite) (Spandler et al., 2011; Angiboust et al., 2014; Vitale Brovarone et al., 2014; Fornash & Whitney, 2020). In addition, the solubility of Cr can be significantly enhanced in Cl-rich, saline fluids (Huang et al., 2019), the compositions of which resemble serpentinite-derived fluids (Scambelluri et al., 2004; Kendrick et al., 2011; Huang et al., 2017).

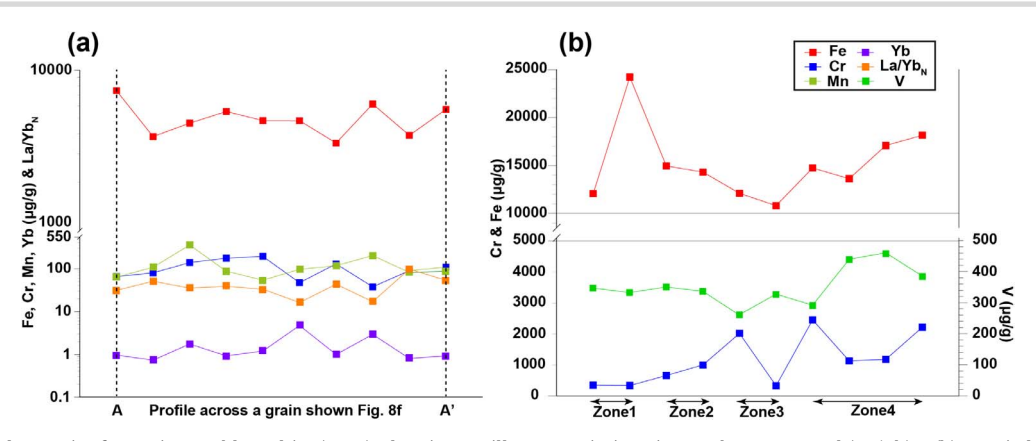


Fig. 16. (a) Matrix lawsonite from Ring Mt blueschist (RR-1), showing oscillatory variations in Fe, Yb, Cr, Mn, and (La/Yb) $_{\rm N}$. (b) Matrix lawsonite from Sivrihisar blueschist (SV01-75A), showing oscillatory variations in Cr, Fe, and V across Zones 3–4.

Serpentinite-sourced fluids can also explain the high bulk Cr and Ni contents of the Sivrihisar blueschist (Table 2).

Variations of Sr/Pb and Cr/V

The Sr/Pb ratio in lawsonite varies as a function of rock type; lawsonite in metabasite tends to have higher Sr/Pb than lawsonite in quartz-rich metasediment regardless of the occurrence and variable modes of Sr- and/or Pbbearing phases (e.g. titanite, apatite, epidote) (Martin et al., 2011; Fornash et al., 2019; Whitney et al., 2020). For instance, matrix grains from a Guatemala eclogite that underwent metasomatic alteration by metasedimentsourced fluids (Hara et al., 2018) record Sr/Pb between those from less-altered eclogite and metachert in the same region (Fig. 10a). Possible Pb-bearing titanite only occurs in the metasomatized eclogite and the metachert (Hara et al., 2018). Our compilation of lawsonite composition suggests that lawsonite in calcschist has Sr/Pb mostly higher than lawsonite in quartz-rich metasediment but within the range of lawsonite in metabasite (Supplementary Table S1).

As with Sr/Pb, the Cr concentration of lawsonite correlates with rock type. In general, lawsonite in quartz-rich metasediment contains lower Cr concentrations than lawsonite in metabasite despite the lower abundance of Cr-bearing competitors (e.g. garnet) in metasediment (Supplementary Table S1). Lawsonite that interacted with serpentinite/metagabbro is enriched in Cr and Ni contents (Angiboust et al., 2014; Vitale Brovarone et al., 2014; Fornash & Whitney, 2020). The V contents of lawsonite in quartz-rich metasediment, calcschist, and metabasite overlap each other (Supplementary Table S1), and they tend to correlate with the Cr contents positively (Fig. 10e).

Consequently, Sr/Pb and Cr/V ratios of lawsonite are useful to evaluate the control of host rock signatures. Sr/Pb_{Bulk} and Cr/V_{Bulk} were additionally calculated relative to bulk-rock ratios of matrix even for vein-associated lawsonite. Significant deviations from the bulk-rock ratios (e.g. $\text{Cr/V}_{\text{Bulk}} > 1$) would provide additional information on (1) the timing of specific element

exchanges (e.g. Cr-enrichment), (2) element fractionation with coexisting minerals, and/or (3) changes in mineral modes (excluding lawsonite). The element concentrations of lawsonite that vary at a consistent rate (e.g. constant Sr/Pb, Sr/Pb_{Bulk}) would indicate modal changes in lawsonite because element ratios of lawsonite are not affected by lawsonite mode.

Lawsonite grains in the Franciscan metabasalts show noticeable differences in Sr/Pb_{Bulk} and/or Cr/V_{Bulk} depending on their textural locations (vein vs. host matrix). In the N Berkeley Hills blueschist (EC-1B) and the Ring Mt blueschist/eclogite (LVT-1), vein-lawsonite is higher in Cr/V_{Bulk} (>1) than matrix lawsonite (\leq 1), with a lower-to-similar range of Sr/Pb_{Bulk} (Fig. 17a). The higher Cr/V_{Bulk} of vein-lawsonite stems from significantly higher Cr_{Bulk} compared with matrix lawsonite (Fig. 17b). In conjunction with the high Cr_{Bulk} of vein-lawsonite, the vein area of sample EC-1B has bulk Cr content higher than the matrix (Table 2), suggesting the Cr-rich nature of vein-forming fluids. The vein-lawsonite in sample LVT-1 displays a gradual Cr/V_{Bulk} decrease from Zone 2 to Zone 3 due to a significant Cr_{Bulk} decrease (blueschist layer) or increasing V_{Bulk} (eclogite layer) (Fig. 17b). This contrasts with the matrix lawsonite in blueschist layers that shows less Cr_{Bulk} and V_{Bulk} variations (Fig. 17b). These variations in Zones 2 and 3 indicate that Cr- and V-partitioning was not crystallographically controlled. Possible mechanisms for the variable partitioning include compositional changes in infiltrating fluids (e.g. V-poor to -rich veinforming fluids in eclogite layers) and/or changes in mineral modes and assemblages. The vein-lawsonite with high Cr/V_{Bulk} has Sr/Pb corresponding to the range of lawsonite in metabasite (>30; Fig. 10b-d) and its Sr/Pb is higher than the bulk Sr/Pb of the host matrix $(Sr/Pb_{Bulk} > 1; Fig. 17a)$. The likely source of Sr/Pb- and Cr-rich vein-forming fluids are (meta)ultramafic rocks.

On the other hand, lawsonite grains in the calcite-rich vein of the Ring Mt blueschist (RR-1) have Sr/Pb_{Bulk} lower than that of matrix lawsonite, with Sr/Pb comparable with lawsonite in calcschist-to-metabasite (Figs 10c and 17a). The relatively low Sr/Pb_{Bulk} of vein-lawsonite is attributable to Sr/Pb-fractionation with Sr/Pb-hosting

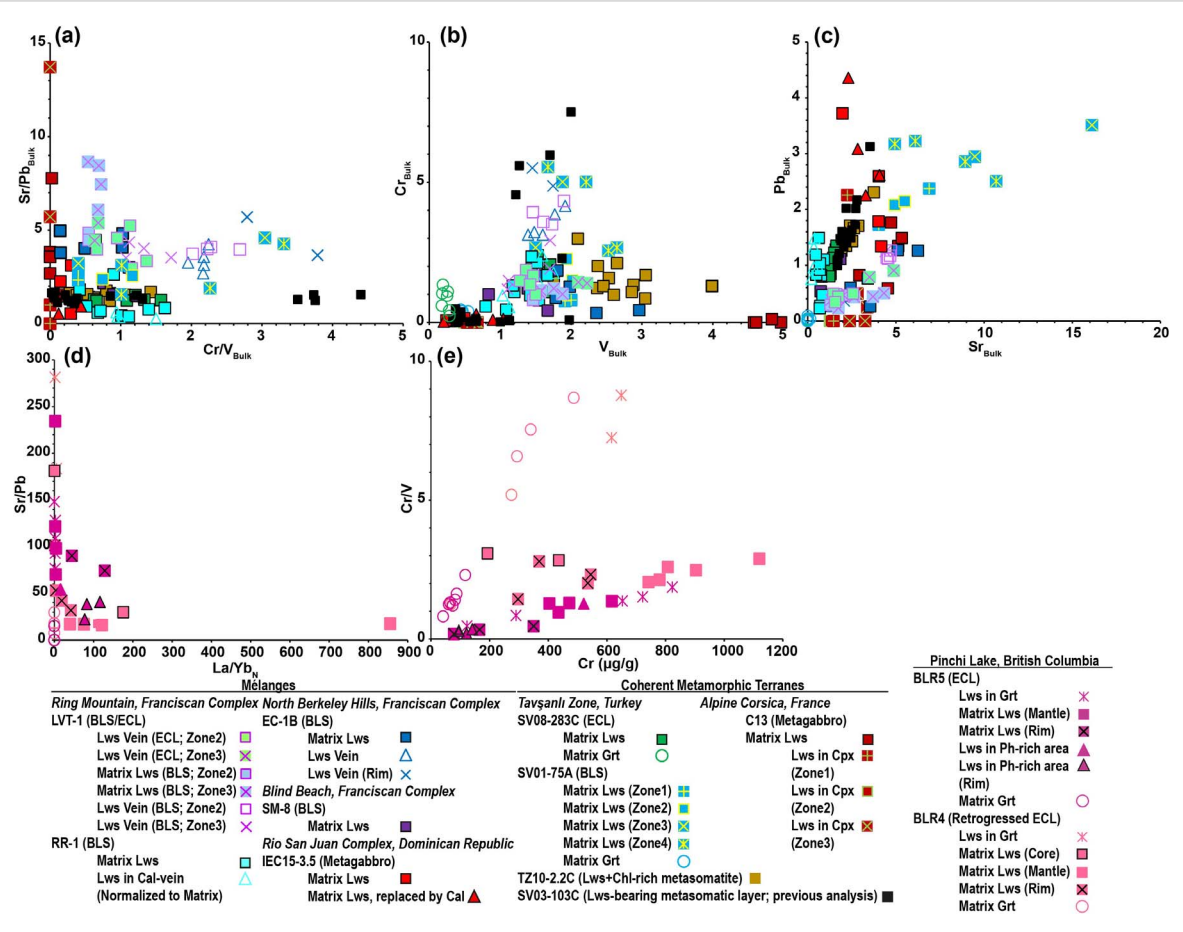


Fig. 17. (a) Sr/Pb_{Bulk} vs. Cr/V_{Bulk}. (b) Cr_{Bulk} vs. V_{Bulk}. (c) Pb_{Bulk} vs. Sr_{Bulk}. (d, e) Sr/Pb vs. (La/Yb)_N (d) and Cr/V vs. Cr (e) in lawsonite from the Pinchi Lake eclogites (BLR4, 5).

calcite (Table 1). It is also likely that the vein-forming fluids were Sr/Pb-poorer than the host matrix; bulkrock measurements support this interpretation (vein: 131; host matrix: 151 Sr/Pb). Together with the lower Sr/Pb, the vein has higher bulk LREE and lower Ni and Cr contents than the host matrix (Figs 5 and 6). These compositional characteristics suggest that vein-forming fluids were likely derived from (meta)sediment, such as

Matrix grains from the Sivrihisar eclogite (SV08-283C) and the Tavşanlı metasomatite (TZ10-2.2C) are characterized by variable Cr/V_{Bulk} and consistent Sr/Pb_{Bulk} (Fig. 17a). Only the grains from the Sivrihisar blueschist (SV01-75A) show changes in both Sr/Pb_{Bulk} and Cr/V_{Bulk} (Fig. 17a). The Cr/V_{Bulk} variations could arise from interactions with Cr/V-rich or -poor fluids and/or Cr/Vfractionations with coexisting minerals. Matrix garnet in the Sivrihisar blueschist and eclogite (SV01-75A, SV08-283C) is one of major host minerals of Cr (Fig. 13c), so Cr-fractionation with garnet cannot explain high Cr_{Bulk} and Cr/V_{Bulk} (>1) in matrix lawsonite. For instance, Zones 3 and 4 of matrix lawsonite in the blueschist records Cr/V_{Bulk} significantly higher than that of associated Zones 1 and 2 (0.4-3.31 vs. 0.40-1.17) and coexisting matrix garnet (0.51–1.05) but comparable with the range of lawsonite in metasomatic layers that developed at the

margins of eclogite pods in the same region (Fig. 17a). Fornash & Whitney et al. (2020) proposed that these layers obtained Ni and Cr by the influx of external fluids sourced from (meta)ultramafic rocks. The Sivrihisar blueschist might have been influenced by similar fluids, as evidenced by the high Cr_{Bulk} and Cr/V_{Bulk} in matrix lawsonite comparable with metasomatic lawsonite (Fig. 17a and b), Cr-oscillatory zoning in matrix lawsonite (Fig. 8e), and the bulk Ni and Cr enrichment of matrix blueschist (Table 2). From Zones 1 and 2 to Zones 3 and 4, Sr/Pb_{Bulk} increases with Cr/V_{Bulk} (Fig. 17a) and matrix lawsonite has Sr/Pb corresponding to lawsonite in metabasite (>30) (Fig. 10a). These features further support the influence of (meta)ultramafic rocks. Relative to the Sivrihisar metabasalts, the Tavşanlı metasomatite is higher in bulk V content, but lower in bulk Cr content (Fig. 5). Matrix lawsonite in this metasomatite significantly hosts bulk V (Fig. 13c) shows wider variations in V_{Bulk} than Cr_{Bulk} (Fig. 17b) and has Sr/Pb within the range of metabasite (Fig. 10a). This indicates possible interactions with V-rich (thus Cr/Vpoor) fluids potentially sourced from metabasite during metasomatic alteration.

Lawsonite in metagabbro (C13, IEC15-3.5) has the lowest range of Cr/V_{Bulk} and the widest range of Sr/Pb_{Bulk} among the analyzed grains (Fig. 17a). This is mainly

because of the extremely low Cr_{Bulk} and significant variations in Pb_{Bulk} and Sr_{Bulk} (Fig. 17b and c). Amphibole in IEC15-3.5 and clinopyroxene in C13 contain up to 727 and 278 Cr μ g/g, respectively (Supplementary Table S1), and their modal abundances are significantly high in the host matrix (Table 1). These matrix minerals, thus, might have fractionated Cr from coexisting lawsonite (Spandler et al., 2011; Angiboust et al., 2014). In addition, the low bulk Cr content in C13 could contribute to the low Cr/V_{Bulk} (Fig. 5; Table 2). Element fractionation with Sr- and/or Pb-bearing phases (e.g. calcite, epidote; Table 1) likely induced Sr/Pb_{Bulk} variations, as evidenced by the lower Sr/Pb_{Bulk} of lawsonite partially replaced by calcite (0.53-1.55; Fig. 3j) compared with lawsonite with no textural replacement (0.53–3.11; e.g. IEC15-3.5) (Fig. 17a). This element fractionation might have varied in response to modal changes in Sr- and/or Pb-bearing minerals, in which case, caused additional Sr/PbBulk variations. Lawsonite in the partially replaced domains of omphacite (C13) records a higher range of Sr/Pb_{Bulk} than matrix lawsonite, possibly indicating the Pb-poor (thus Sr/Pb-rich) nature of infiltrating fluids (Fig. 17a and c).

In the Pinchi Lake eclogites, matrix lawsonite in the more retrogressed sample (BLR4) shows a clear correlation between Sr/Pb and LREE contents; LREE contents initially increase and subsequently decrease, whereas Sr/Pb decreases and then increases toward the Fe-rich rims (Fig. 17d). We interpreted that the initial changes in LREE and Sr/Pb likely resulted from interactions with quartzbearing (meta)sediment. Similar (meta)sedimentary signatures are recorded at the rims of lawsonite grains in the matrix and the phengite-rich area of less retrogressed sample (BLR5) (Fig. 17d). These grains in BLR5 display noticeable Cr depletion and decreasing Cr/V, which are in accordance with the (meta)sedimentary signatures (Fig. 17e). In contrast to the BLR5 grains, initial LREE enrichment is accompanied by Cr enrichment in matrix BLR4 grains (Fig. 17d and e), likely owing to Cr variations induced by lawsonite modal changes given the consistent Cr/V (Fig. 17e). The subsequent changes in LREE and Sr/Pb are only observed in matrix lawsonite from the more retrogressed BLR4 (Fig. 17d). Lawsonite inclusions in garnet are significantly depleted in L-MREE (Fig. 9c and d) and have Cr/V within the range of host garnet (Fig. 17e). In particular, the BLR4 inclusion records noticeably high Cr/V (Fig. 17e), with high Sr/Pb corresponding to lawsonite in metabasite (>30; Fig. 17d). These features might have originated from Cr/V and Sr/Pb-rich fluids released during serpentinization, which was interpreted to be contemporaneous with blueschistfacies metamorphism of metabasaltic units (Paterson, 1977).

IMPLICATIONS AND CONCLUSION

This study shows that the composition and zoning of lawsonite is a useful indicator of fluid-rock interaction during subduction metamorphism, although care must

be taken to understand the mechanisms controlling lawsonite composition and its variation. Vein-lawsonite from Franciscan metabasites records low Sr/Pb or high Cr/V, reflecting various sources of vein-forming fluids ((meta)sediment, serpentinite/metagabbro). Lawsonite in metasomatized domains (e.g. replaced domains of omphacite in Corsica metagabbro) differs in Sr/Pb or Cr/V from matrix lawsonite, suggesting the compositional characteristics of infiltrating fluids. The bulk LILE, LREE, and/or Th enrichments of most metabasites (except from Corsica) and the Tayşanlı metasomatite indicate possible interactions with (meta)sediment, although the composition of matrix lawsonite records no such signatures. Instead, matrix lawsonite shows compositional variations in REE, TEs, and element ratios (Sr/Pb, Cr/V) that suggest (1) element fractionation between minerals, (2) the influence of crystallographic control (i.e. in Ti-sector zoning), and/or (3) intermittent interactions with fluids sourced from (meta)mafic-toultramafic rocks. Only a few grains preserve possible sedimentary signatures in their cores (e.g. low Sr/Pb). This inconsistency might be related to the timing of interaction with (meta)sediments that likely occurred prior to or at the early stages of lawsonite growth. In this case, matrix lawsonite inherited (meta)sedimentinfluenced signatures from its host rock, and its compositional variations only record the changes that occurred during its growth. This hypothesis could be tested if advances are made in lawsonite geochronology.

Our study shows that lawsonite is an effective recorder of elemental redistributions driven by various stages of mineral reactions and fluid-rock interactions in subduction systems. To track element transfer history during subduction metamorphism, it is important to document lawsonite and its host rock compositions and to evaluate compositional zoning patterns.

DATA AVAILABILITY STATEMENT

The data are available in online supplementary material.

SUPPLEMENTARY DATA

Supplementary data are available at Journal of Petrology online.

ACKNOWLEDGEMENTS

We would like to thank Stacia Gordon, Edward Ghent, Sean Mulcahy, and Alberto Vitale Brovarone for generously providing samples from Dominican Republic, British Columbia, Franciscan Complex, and Alpine Corsica, respectively. We also gratefully acknowledge John Wakabayashi, Mario Alfredo Ramos Arias, and Jessie Shields for their valuable help in collecting samples from the Franciscan Complex. We are grateful for thorough reviews by Jörg Hermann, Samuel Angiboust, Tatsuki Tsujimori, and an anonymous reviewer, which improved the quality of this manuscript. This work was funded by

the University of Minnesota (Grant-in-Aid program) and NSF grant EAR-1949895 to D.L.W.

References

- Agard, P., Monié, P., Gerber, W., Omrani, J., Molinaro, M., Meyer, B., Labrousse, L., Vrielynck, B., Jolivet, L. & Yamato, P. (2006). Transient, synobduction exhumation of Zagros blueschists inferred from P-T, deformation, time, and kinematic constraints: implications for Neotethyan wedge dynamics. Journal of Geophysical Research 111, B11401. https://doi.org/10.1029/2005JB004103.
- Angiboust, S., Agard, P., Glodny, J., Omrani, J. & Oncken, O. (2016). Zagros blueschists: episodic underplating and long-lived cooling of a subduction zone. Earth and Planetary Science Letters 443, 48-58. https://doi.org/10.1016/j.epsl.2016.03.017.
- Angiboust, S., Pettke, T., De Hoog, J. C. M., Caron, B. & Oncken, O. (2014). Channelized fluid flow and eclogite-facies metasomatism along the subduction shear zone. Journal of Petrology 55, 883-916. https:// doi.org/10.1093/petrology/egu010.
- Becker, H., Jochum, K. P. & Carlson, R. W. (2000). Trace element fractionation during dehydration of eclogites from high-pressure terranes and the implications for element fluxes in subduction zones. Chemical Geology 163, 65-99. https://doi.org/10.1016/ S0009-2541(99)00071-6.
- Blake, M. C., Jr. (1988). Metamorphic and tectonic evolution of the Franciscan Complex, northern California. Metamorphism and crustal evolution of the Western United States 38, 1035-1060.
- Brothers, R. N. (1954). Glaucophane schists from the North Berkeley Hills, California. American Journal of Science 252, https://doi. org/10.2475/ajs.252.10.614.
- Catlos, E. J. (2003). Phengite-based chronology of K- and Ba-rich fluid flow in two Paleosubduction zones. Science 299, 92–95. https://doi. org/10.1126/science.1076977.
- Çetinkaplan, M., Candan, O., Oberhänsli, R. & Bousquet, R. (2008). Pressure-temperature evolution of lawsonite eclogite in Sivrihisar; Tavşanlı Zone-Turkey. Lithos 104, 12-32. https://doi. org/10.1016/j.lithos.2007.11.007.
- Coleman, R. G. & Lanphere, M. A. (1971). Distribution and age of highgrade blueschists, associated eclogites, and amphibolites from Oregon and California. GSA Bulletin 82, 2397-2412. https://doi. org/10.1130/0016-7606(1971)82[2397:DAAOHB]2.0.CO;2.
- Cruz-Uribe, A. M., Page, F. Z., Lozier, E., Feineman, M. D., Zack, T., Mertz-Kraus, R., Jacob, D. E. & Kitajima, K. (2021). Trace element and isotopic zoning of garnetite veins in amphibolitized eclogite, Franciscan Complex, California, USA. Contributions to Mineralogy and Petrology 176, 41. https://doi.org/10.1007/ s00410-021-01795-4.
- Davis, P. B. & Whitney, D. L. (2006). Petrogenesis of lawsonite and epidote eclogite and blueschist, Sivrihisar Massif, Turkey. Journal of Metamorphic Geology 24, 823-849. https://doi.org/10.1111/ j.1525-1314.2006.00671.x.
- Davis, P. B. & Whitney, D. L. (2008). Petrogenesis and structural petrology of high-pressure metabasalt pods, Sivrihisar, Turkey. Contributions to Mineralogy and Petrology 156, 217-241. https://doi. org/10.1007/s00410-008-0282-4.
- Deschamps, F., Godard, M., Guillot, S. & Hattori, K. (2013). Geochemistry of subduction zone serpentinites: a review. Lithos 178, 96-127. https://doi.org/10.1016/j.lithos.2013.05.019.
- Deschamps, F., Guillot, S., Godard, M., Andreani, M. & Hattori, K. (2011). Serpentinites act as sponges for fluid-mobile elements in abyssal and subduction zone environments. Terra Nova 23, 171-178. https://doi.org/10.1111/j.1365-3121.2011.00995.x.

- Dumitru, T. A., Ernst, W. G., Hourigan, J. K. & McLaughlin, R. J. (2015). Detrital zircon U-Pb reconnaissance of the Franciscan subduction complex in northwestern California. International Geology Review 57, 767–800. https://doi. org/10.1080/00206814.2015.1008060.
- Dumitru, T. A., Ernst, W. G., Wright, J. E., Wooden, J. L., Wells, R. E., Farmer, L. P., Kent, A. J. R. & Graham, S. A. (2013). Eocene extension in Idaho generated massive sediment floods into the Franciscan trench and into the Tyee, Great Valley, and Green River basins. Geology 41, 187-190. https://doi.org/10.1130/G33746.1.
- Elliott, T. (2003) Tracers of the slab. In: Eiler, J. (ed.). In: Inside the Subduction Factory. American Geophysical Union, Geophysical Monograph 138, pp.23-45. Washington, District of Columbia, USA: American Geophysical Union.
- Endo, S., Wallis, S. R., Tsuboi, M., Torres De León, R. & Solari, L. A. (2012). Metamorphic evolution of lawsonite eclogites from the southern Motagua fault zone, Guatemala: insights from phase equilibria and Raman spectroscopy. Journal of Metamorphic Geology 30, 143-164. https://doi.org/10.1111/j.1525-1314.2011.00960.x.
- Ernst, W. G. (2011). Accretion of the Franciscan Complex attending Jurassic-Cretaceous geotectonic development of northern and central California. GSA Bulletin 123, 1667-1678. https://doi. org/10.1130/B30398.1.
- Ernst, W. G. & Liu, J. (1998). Experimental phase-equilibrium study of Al- and Ti-contents of calcic amphibole in MORB; a semiquantitative thermobarometer. American Mineralogist 83, 952-969. https:// doi.org/10.2138/am-1998-9-1004.
- Escuder-Viruete, J. & Pérez-Estaún, A. (2006). Subduction-related P-T path for eclogites and garnet glaucophanites from the Samaná Peninsula basement complex, northern Hispaniola. International Journal of Earth Sciences 95, 995-1017. https://doi.org/10.1007/ s00531-006-0079-5.
- Escuder-Viruete, J., Pérez-Estaún, A., Gabites, J. & Suárez-Rodríguez, Á. (2011). Structural development of a high-pressure collisional accretionary wedge: the Samaná complex, Northern Hispaniola. Journal of Structural Geology 33, 928-950. https://doi.org/10.1016/j. jsg.2011.02.006.
- Escuder-Viruete, J., Valverde-Vaquero, P., Rojas-Agramonte, Y., Jabites, J. & Pérez-Estaún, A. (2013). From intra-oceanic subduction to arc accretion and arc-continent collision: insights from the structural evolution of the Río San Juan metamorphic complex, northern Hispaniola. Journal of Structural Geology 46, 34-56. https://doi. org/10.1016/j.jsg.2012.10.008.
- Fornash, K. F., Cosca, M. A. & Whitney, D. L. (2016). Tracking the timing of subduction and exhumation using 40 Ar/39 Ar phengite ages in blueschist- and eclogite-facies rocks (Sivrihisar, Turkey). Contributions to Mineralogy and Petrology 171, 67. https://doi.org/10.1007/ s00410-016-1268-2.
- Fornash, K. F. & Whitney, D. L. (2020). Lawsonite-rich layers as records of fluid and element mobility in subducted crust (Sivrihisar Massif, Turkey). Chemical Geology 533, 119356. https://doi.org/10.1016/ j.chemgeo.2019.119356.
- Fornash, K. F., Whitney, D. L. & Seaton, N. C. A. (2019). Lawsonite composition and zoning as an archive of metamorphic processes in subduction zones. Geosphere 15, 24–46. https://doi.org/10.1130/
- Forneris, J. F. & Holloway, J. R. (2003). Phase equilibria in subducting basaltic crust: implications for H₂O release from the slab. Earth and Planetary Science Letters 214, 187–201. https://doi.org/10.1016/ S0012-821X(03)00305-4.
- Gale, A., Dalton, C. A., Langmuir, C. H., Su, Y. & Schilling, J. G. (2013). The mean composition of ocean ridge basalts. Geochemistry, Geophysics, Geosystems 14, https://doi.org/10.1029/2012GC004334.

- Ghent, E., Tinkham, D. & Marr, R. (2009). Lawsonite eclogites from the Pinchi Lake area, British Columbia—new P-T estimates and interpretation. Lithos 109, 248-253. https://doi.org/10.1016/j. lithos.2008.06.018.
- Ghent, E. D., Erdmer, P., Archibald, D. A. & Stout, M. Z. (1996). Pressure-temperature and tectonic evolution of Triassic lawsonitearagonite blueschists from Pinchi Lake, British Columbia. Canadian Journal of Earth Sciences 33, 800-810. https://doi.org/10.1139/ e96-061.
- Ghent, E. D., Stout, M. Z. & Erdmer, P. (1993). Pressure-temperature evolution of lawsonite-bearing eclogites, Pinchi Lake, British Columbia. Journal of Metamorphic Geology 11, 279-290. https://doi. org/10.1111/j.1525-1314.1993.tb00147.x.
- Giaramita, M. J. & Sorensen, S. S. (1994). Primary fluids in lowtemperature eclogites: evidence from two subduction complexes (Dominican Republic, and California, USA). Contributions to Mineralogy and Petrology 117, 279-292. https://doi.org/10.1007/
- Hacker, B. R., Peacock, S. M., Abers, G. A. & Holloway, S. D. (2003). Subduction factory 2. Are intermediate-depth earthquakes in subducting slabs linked to metamorphic dehydration reactions? Journal of Geophysical Research 108, 2030.
- Hara, T., Tsujimori, T., Chang, Q. & Kimura, J. I. (2018). In-situ Sr-Pb isotope geochemistry of lawsonite: a new method to investigate slab-fluids. Lithos 320-321, 93-104. https://doi.org/10.1016/j. lithos.2018.09.001.
- Harlow, G. E., Sisson, V. B., Avé Lallemant, H. G., Sorensen, S. S. & Seitz, R. (2003). High-pressure metasomatic rocks along the Motagua Fault Zone, Guatemala. Ofioliti 28, 115-120.
- Huang, J., Hao, J., Huang, F. & Sverjensky, D. A. (2019). Mobility of chromium in high temperature crustal and upper mantle fluids. Geochemical Perspectives Letters 12, 1-6. https://doi.org/10.7185/ geochemlet.1926.
- Huang, R., Sun, W., Zhan, W., Ding, X., Zhu, J. & Liu, J. (2017). Influence of temperature, pressure, and fluid salinity on the distribution of chlorine into serpentine minerals. Journal of Asian Earth Sciences 145, 101-110. https://doi.org/10.1016/j.jseaes.2017.04.022.
- John, T., Klemd, R., Gao, J. & Garbe-Schönberg, C. D. (2008). Traceelement mobilization in slabs due to non steady-state fluidrock interaction: constraints from an eclogite-facies transport vein in blueschist (Tianshan, China). Lithos 103, 1-24. https://doi. org/10.1016/j.lithos.2007.09.005.
- Kang, P., Fornash, K. F. & Whitney, D. L. (2020). Controls on development of different mineral assemblages in gabbro and basalt during subduction metamorphism. Contributions to Mineralogy and Petrology 175, 113. https://doi.org/10.1007/s00410-020-01753-6.
- van Keken, P. E., Hacker, B. R., Syracuse, E. M. & Abers, G. A. (2011). Subduction factory: 4. Depth-dependent flux of H₂O from subducting slabs worldwide. Journal of Geophysical Research 116,
- Kendrick, M. A., Scambelluri, M., Honda, M. & Phillips, D. (2011). High abundances of noble gas and chlorine delivered to the mantle by serpentinite subduction. Nature Geoscience 4, 807–812. https://doi. org/10.1038/ngeo1270.
- Krebs, M., Maresch, W. V., Schertl, H. P., Münker, C., Baumann, A., Draper, G., Idleman, B. & Trapp, E. (2008). The dynamics of intraoceanic subduction zones: a direct comparison between fossil petrological evidence (Rio San Juan Complex, Dominican Republic) and numerical simulation. Lithos 103, 106-137. https://doi. org/10.1016/j.lithos.2007.09.003.
- Krebs, M., Schertl, H. P., Maresch, W. V. & Draper, G. (2011). Mass flow in serpentinite-hosted subduction channels: P-T-t path patterns

- of metamorphic blocks in the Rio San Juan mélange (Dominican Republic). Journal of Asian Earth Sciences 42, 569-595. https://doi. org/10.1016/j.jseaes.2011.01.011.
- Krogh, E. J., Oh, C. W. & Liou, J. C. (1994). Polyphase and anticlockwise P-T evolution for Franciscan eclogites and blueschists from Jenner, California, USA. Journal of Metamorphic Geology 12, 121–134. https://doi.org/10.1111/j.1525-1314.1994.tb00008.x.
- Lagabrielle, Y. & Lemoine, M. (1997). Alpine, Corsican and Apennine ophiolites: the slow-spreading ridge model. Earth and Planetary Science 325, 909-920.
- Lefeuvre, B., Agard, P., Verlaguet, A., Dubacq, B. & Plunder, A. (2020). Massive formation of lawsonite in subducted sediments from the Schistes Lustrés (W. Alps): implications for mass transfer and decarbonation in cold subduction zones. Lithos 370-371, 105629. https://doi.org/10.1016/j.lithos.2020.105629.
- Martin, L. A. J., Hermann, J., Gauthiez-Putallaz, L., Whitney, D. L., Vitale Brovarone, A., Fornash, K. F. & Evans, N. J. (2014). Lawsonite geochemistry and stability-implication for trace element and water cycles in subduction zones. Journal of Metamorphic Geology 32, 455-478. https://doi.org/10.1111/jmg.12093.
- Martin, L. A. J., Rubatto, D., Vitale Brovarone, A. & Hermann, J. (2011). Late Eocene lawsonite-eclogite facies metasomatism of a granulite sliver associated to ophiolites in Alpine Corsica. Lithos 125, 620-640. https://doi.org/10.1016/j.lithos.2011.03.015.
- Meresse, F., Lagabrielle, Y., Malavieille, J. & Ildefonse, B. (2012). A fossil ocean-continent transition of the Mesozoic Tethys preserved in the Schistes Lustrés nappe of northern Corsica. Tectonophysics 579, 4-16. https://doi.org/10.1016/j.tecto.2012.06.013.
- Mevel, C. & Kienast, J. R. (1980). Chromian jadeite, phengite, pumpellyite, and lawsonite in a high-pressure metamorphosed gabbro from the French Alps. Mineralogical Magazine 43, 979–984. https:// doi.org/10.1180/minmag.1980.043.332.04.
- Molli, G., Tribuzio, R. & Marquer, D. (2006). Deformation and metamorphism at the eastern border of the Tenda Massif (NE Corsica): a record of subduction and exhumation of continental crust. Journal of Structural Geology 28, 1748-1766. https://doi.org/10.1016/ j.jsg.2006.06.018.
- Mulcahy, S. R., Vervoort, J. D. & Renne, P. R. (2014). Dating subductionzone metamorphism with combined garnet and lawsonite Lu-Hf geochronology. Journal of Metamorphic Geology 32, 515–533. https:// doi.org/10.1111/jmg.12092.
- Muñoz-Montecinos, J., Angiboust, S., Garcia-Casco, A., Glodny, J. & Bebout, G. (2021). Episodic hydrofracturing and large-scale flushing along deep subduction interfaces: implications for fluid transfer and carbon recycling (Zagros Orogen, southeastern Iran). Chemical Geology 571, 120173. https://doi.org/10.1016/j. chemgeo.2021.120173.
- Nutman, A. P., Buckman, S., Hidaka, H., Kamiichi, T., Belousova, E. & Aitchison, J. (2013). Middle Carboniferous-Early Triassic eclogite-blueschist blocks within a serpentinite mélange at Port Macquarie, eastern Australia: implications for the evolution of Gondwana's eastern margin. Gondwana Research 24, 1038–1050. https://doi.org/10.1016/j.gr.2013.01.009.
- Och, D. J., Leitch, E. C., Caprarelli, G. & Watanabe, T. (2003). Blueschist and eclogite in tectonic mélange, Port Macquarie, New South Wales, Australia. Mineralogical Magazine 67, 609-624. https://doi. org/10.1180/0026461036740121.
- Okay, A. I. & Kelley, S. P. (1994). Tectonic setting, petrology and geochronology of jadeite glaucophane and chloritoid glaucophane schists from north-west Turkey. Journal of Metamorphic Geology 12, 455-466. https://doi.org/10.1111/j.1525-1314.1994. tb00035.x.

- Okay, A. I. & Whitney, D. L. (2010). Blueschists, ophiolites and suture zones in northwest Turkey: a review and a field excursion guide. Ofioliti 35, 131-172.
- Page, F. Z., Armstrong, L. S., Essene, E. J. & Mukasa, S. B. (2007). Prograde and retrograde history of the junction school eclogite, California, and an evaluation of garnet-phengite-clinopyroxene thermobarometry. Contributions to Mineralogy and Petrology 153, 533-555. https://doi.org/10.1007/s00410-006-0161-9.
- Palme, H. & O'Neill, H. (2007). Cosmochemical estimates of mantle composition. Treatise on Geochemistry, 1-38. https://doi. org/10.1016/B0-08-043751-6/02177-0.
- Paterson, I. A. (1973) Geology of the Pinchi Lake area, central British Columbia. Dissertation. Vancouver, CA: University of British
- Paterson, I. A. (1977). The geology and evolution of the Pinchi Fault Zone at Pinchi Lake, central British Columbia. Canadian Journal of Earth Sciences 14, 1324-1342. https://doi.org/10.1139/e77-120.
- Paterson, I. A. & Harakal, J. E. (1974). Potassium-argon dating of blueschists from Pinchi Lake, Central British Columbia. Canadian Journal of Earth Sciences 11, 1007-1011. https://doi.org/10.1139/ e74-097.
- Pawley, A. R. (1994). The pressure and temperature stability limits of lawsonite: implications for H₂O recycling in subduction zones. Contributions to Mineralogy and Petrology 118, 99-108. https://doi. org/10.1007/BF00310614.
- Pindell, J. L. & Kennan, L. (2009). Tectonic evolution of the Gulf of Mexico, Caribbean and northern South America in the mantle reference frame: an update. Geological Society, London, Special Publications 328, 1-55. https://doi.org/10.1144/SP328.1.
- Plank, T. (2005). Constraints from thorium/lanthanum on sediment recycling at subduction zones and the evolution of the continents. Journal of Petrology 46, 921-944. https://doi.org/10.1093/ petrology/egi005.
- Plank, T. (2014). The chemical composition of subducting sediments. In: Rudnick, R. L. (ed.) Treatise on Geochemistry 4: The Crust. Oxford, UK: Elsevier-Pergamon, 607-629, https://doi.org/10.1016/ B978-0-08-095975-7.00319-3.
- Platt, J. P. (1975). Metamorphic and deformational processes in the Franciscan Complex, California: some insights from the Catalina Schist terrane. GSA Bulletin 86, 1337-1347. 10.1130/0016-7606 (1975)861337:MADPIT2.0.CO;2.
- Plunder, A., Agard, P., Chopin, C. & Okay, A. I. (2013). Geodynamics of the Tavşanlı Zone, western Turkey: insights into subduction/obduction processes. Tectonophysics 608, 884–903. https://doi. org/10.1016/j.tecto.2013.07.028.
- Poli, S. & Schmidt, M. W. (1995). H₂O transport and release in subduction zones: experimental constraints on basaltic and andesitic systems. Journal of Geophysical Research 100, 22299-22314. https:// doi.org/10.1029/95JB01570.
- Pourteau, A., Scherer, E. E., Schorn, S., Bast, R., Schmidt, A. & Ebert, L. (2019). Thermal evolution of an ancient subduction interface revealed by Lu-Hf garnet geochronology, Halilbağı Complex (Anatolia). Geoscience Frontiers 10, 127-148. https://doi.org/10.1016/j. gsf.2018.03.004.
- Ravna, E. J. K., Andersen, T. B., Jolivet, L. & de Capitani, C. (2010). Cold subduction and the formation of lawsonite eclogiteconstraints from prograde evolution of eclogitized pillow lava from Corsica. Journal of Metamorphic Geology 28, 381-395. https:// doi.org/10.1111/j.1525-1314.2010.00870.x.
- de Roever, W. P. & Brothers, R. N. (1955). Glaucophane schists from the North Berkeley Hills, California; discussion and reply. American Journal of Science 253, 240-246. https://doi.org/10.2475/ ajs.253.4.240.

- Ryan, J. G., Morris, J., Tera, F., Leeman, W. P. & Tsvetkov, A. (1995). Cross-arc geochemical variations in the Kurile Arc as a function of slab depth. Science 270, 625-627. https://doi.org/10.1126/ science.270.5236.625.
- Scambelluri, M., Bottazzi, P., Trommsdorff, V., Vannucci, R., Hermann, J., Gòmez-Pugnaire, M. T. & Lòpez-Sànchez Vizcaìno, V. (2001). Incompatible element-rich fluids released by antigorite breakdown in deeply subducted mantle. Earth and Planetary Science Letters 192, 457-470. https://doi.org/10.1016/S0012-821X(01)00457-5.
- Scambelluri, M., Fiebig, J., Malaspina, N., Müntener, O. & Pettke, T. (2004). Serpentinite subduction: implications for fluid processes and trace-element recycling. International Geology Review 46, 595-613. https://doi.org/10.2747/0020-6814.46.7.595.
- Schmidt, M. W. & Poli, S. (1998). Experimentally based water budgets for dehydrating slabs and consequences for arc magma generation. Earth and Planetary Science Letters 163, 361-379. https://doi. org/10.1016/S0012-821X(98)00142-3.
- Sherlock, S. C. & Okay, A. I. (1999). Oscillatory zoned chrome lawsonite in the Tavşanlı Zone, northwest Turkey. Mineralogical Magazine 63, 687-692. https://doi.org/10.1180/minmag.1999.063.5.06.
- Shervais, J. W. (1982). Ti-V plots and the petrogenesis of modern and ophiolitic lavas. Earth and Planetary Science Letters 59, 101–118. https://doi.org/10.1016/0012-821X(82)90120-0.
- Simons, K. K., Harlow, G. E., Brueckner, H. K., Goldstein, S. L., Sorensen, S. S., Hemming, N. G. & Langmuir, C. H. (2010). Lithium isotopes in Guatemalan and Franciscan HP-LT rocks: insights into the role of sediment-derived fluids during subduction. Geochimica et Cosmochimica Acta 74, 3621-3641. https://doi.org/10.1016/j. gca.2010.02.033.
- Spandler, C., Hermann, J., Arculus, R. & Mavrogenes, J. (2003). Redistribution of trace elements during prograde metamorphism from lawsonite blueschist to eclogite facies; implications for deep subduction-zone processes. Contributions to Mineralogy and Petrology 146, 205-222. https://doi.org/10.1007/s00410-003-0495-5.
- Spandler, C., Pettke, T. & Rubatto, D. (2011). Internal and external fluid sources for eclogite-facies veins in the Monviso metaophiolite, Western Alps: implications for fluid flow in subduction zones. Journal of Petrology 52, 1207–1236. https://doi.org/10.1093/ petrology/egr025.
- Stowell, H., Zuluaga, C., Boyle, A. & Bulman, G. (2011). Garnet sector and oscillatory zoning linked with changes in crystal morphology during rapid growth, North Cascades, Washington. The American Mineralogist 96, 1354–1362. https://doi.org/10.2138/am.2011.3759.
- Sun, S. S. & McDonough, W. F. (1989). Chemical and isotopic systematics of oceanic basalts: implications for mantle composition and processes. Geological Society, London, Special Publications 42, 313–345. https://doi.org/10.1144/GSL.SP.1989.042.01.19.
- Tatsumi, Y. & Eggins, S. (1995) Subduction Zone Magmatism. Oxford, UK: Blackwell Science Oxford, pp. 211.
- Tatsumi, Y., Hamilton, D. L. & Nesbitt, R. W. (1986). Chemical characteristics of fluid phase released from a subducted lithosphere and origin of arc magmas: evidence from high-pressure experiments and natural rocks. Journal of Volcanology and Geothermal Research 29, 293-309. https://doi.org/10.1016/0377-0273(86
- Tenthorey, E. & Hermann, J. (2004). Composition of fluids during serpentinite breakdown in subduction zones: evidence for limited boron mobility. Geology 32, 865. https://doi.org/10.1130/G20610.1.
- Teyssier, C., Whitney, D. L., Toraman, E. & Seaton, N. C. A. (2010). Lawsonite vorticity and subduction kinematics. Geology 38, 1123-1126. https://doi.org/10.1130/G31409.1.

- Tsuchiva, S. & Hirajima, T. (2013). Evidence of the lawsonite eclogite facies metamorphism from an epidote-glaucophane eclogite in the Kotsu area of the Sanbagawa belt, Japan. Journal of Mineralogical and Petrological Sciences 108, 166-171. https://doi.org/10.2465/
- Tsujimori, T., Matsumoto, K., Wakabayashi, J. & Liou, J. G. (2006). Franciscan eclogite revisited: reevaluation of the P-T evolution of tectonic blocks from Tiburon Peninsula, California, U.S.a. Mineralogy and Petrology 88, 243-267. https://doi.org/10.1007/ s00710-006-0157-1.
- Ueno, T. (1999). REE-bearing sector-zoned lawsonite in the Sanbagawa pelitic schists of the eastern Kii Peninsula, central Japan. European Journal of Mineralogy 11, 993-998. 10.1127/ ejm/11/6/0993.
- Usui, T., Kobayashi, K., Nakamura, E. & Helmstaedt, H. (2007). Trace element fractionation in deep subduction zones inferred from a lawsonite-eclogite xenolith from the Colorado Plateau. Chemical Geology 239, 336-351. https://doi.org/10.1016/j. chemgeo.2006.08.009.
- Viete, D. R., Hacker, B. R., Allen, M. B., Seward, G. G. E., Tobin, M. J., Kelley, C. S., Cinque, G. & Duckworth, A. R. (2018). Metamorphic records of multiple seismic cycles during subduction. Science Advances 4, eaaq0234. https://doi.org/10.1126/sciadv.aaq0234.
- Vitale Brovarone, A. (2013). Lawsonite-bearing omphacitites from Alpine Corsica (France). International Journal of Earth Sciences 102, 1377-1379. https://doi.org/10.1007/s00531-013-0901-9.
- Vitale Brovarone, A., Alard, O., Beyssac, O., Martin, L. & Picatto, M. (2014). Lawsonite metasomatism and trace element recycling in subduction zones. Journal of Metamorphic Geology 32, 489-514. https://doi.org/10.1111/jmg.12074.
- Vitale Brovarone, A., Beltrando, M., Malavieille, J., Giuntoli, F., Tondella, E., Groppo, C., Beyssac, O. & Compagnoni, R. (2011a). Inherited ocean-continent transition zones in deeply subducted terranes: insights from Alpine Corsica. Lithos 124, 273-290. https:// doi.org/10.1016/j.lithos.2011.02.013.
- Vitale Brovarone, A., Groppo, C., Hetényi, G., Compagnoni, R. & Malavieille, J. (2011b). Coexistence of lawsonite-bearing eclogite and blueschist: phase equilibria modelling of Alpine Corsica metabasalts and petrological evolution of subducting slabs. Journal of Metamorphic Geology 29, 583-600.
- Wakabayashi, J. (1990). Counterclockwise P-T-t paths from amphibolites, Franciscan Complex, California: relics from the early stages of subduction zone metamorphism. The Journal of Geology 98, 657-680. https://doi.org/10.1086/629432.
- Wakabayashi, J. (1992). Nappes, tectonics of oblique plate convergence, and metamorphic evolution related to 140 million years of continuous subduction, Franciscan Complex, California. The Journal of Geology 100, 19-40. https://doi.org/10.1086/629569.
- Wakabayashi, J. (2015). Anatomy of a subduction complex: architecture of the Franciscan Complex, California, at multiple length and time scales. International Geology Review 57, 669-746. https:// doi.org/10.1080/00206814.2014.998728.
- Wakabayashi, J. & Dumitru, T. A. (2007). 40 Ar/39 Ar ages from coherent, high-pressure metamorphic rocks of the Franciscan Complex, California: revisiting the timing of metamorphism of the world's

- type subduction complex. International Geology Review 49, 873–906. https://doi.org/10.2747/0020-6814.49.10.873.
- Wakabayashi, J., Moores, E. M., Sloan, D. & Stout, D. L. (1999). Subduction and the rock record: concepts developed in the Franciscan Complex, California. Geological Society of America Special Paper 338, 123-133. https://doi.org/10.1130/0-8137-2338-8.123.
- Wass, S. Y. (1973). The origin and petrogenetic significance of hourglass zoning in titaniferous clinopyroxenes. Mineralogical Magazine 39, 133-144. https://doi.org/10.1180/minmag.1973.039.302.01.
- Waters, C. N. (1990). The Cenozoic tectonic evolution of Alpine Corsica. Journal of the Geological Society 147, 811-824. https://doi. org/10.1144/gsjgs.147.5.0811.
- Watson, E. & Liang, Y. (1995). A simple model for sector zoning in slowly grown crystals: implications for growth rate and lattice diffusion, with emphasis on accessory minerals in crustal rocks. The American Mineralogist 80, 1179-1187. https://doi.org/10.2138/ am-1995-11-1209.
- Whitney, D. L. & Davis, P. B. (2006). Why is lawsonite eclogite so rare? Metamorphism and preservation of lawsonite eclogite, Sivrihisar, Turkey. Geology 34, 473-476. https://doi.org/10.1130/G22259.1.
- Whitney, D. L. & Evans, B. W. (2010). Abbreviations for names of rockforming minerals. The American Mineralogist 95, 185-187. https:// doi.org/10.2138/am.2010.3371.
- Whitney, D. L., Fornash, K. F., Kang, P., Ghent, E. D., Martin, L., Okay, A. I. & Vitale Brovarone, A. (2020). Lawsonite composition and zoning as tracers of subduction processes: a global review. Lithos 370-371, 105636. https://doi.org/10.1016/j.lithos.2020.105636.
- Whitney, D. L., Teyssier, C., Seaton, N. C. A. & Fornash, K. F. (2014). Petrofabrics of high-pressure rocks exhumed at the slab-mantle interface from the "point of no return" in a subduction zone (Sivrihisar, Turkey). Tectonics 33, 2315-2341. https://doi. org/10.1002/2014TC003677.
- Wood, D. A. (1980). The application of a Th-Hf-Ta diagram to problems of tectonomagmatic classification and to establishing the nature of crustal contamination of basaltic lavas of the British Tertiary Volcanic Province. Earth and Planetary Science Letters 50, 11-30. https://doi.org/10.1016/0012-821X(80)90116-8.
- Xiao, Y., Niu, Y., Song, S., Davidson, J. & Liu, X. (2013). Elemental responses to subduction-zone metamorphism: constraints from the North Qilian Mountain, NW China. Lithos 160-161, 55-67. https://doi.org/10.1016/j.lithos.2012.11.012.
- You, C. F., Castillo, P. R., Gieskes, J. M., Chan, L. H. & Spivack, A. J. (1996). Trace element behavior in hydrothermal experiments: implications for fluid processes at shallow depths in subduction zones. Earth and Planetary Science Letters 140, 41-52. https://doi. org/10.1016/0012-821X(96)00049-0.
- Zack, T., Rivers, T., Brumm, R. & Kronz, A. (2004). Cold subduction of oceanic crust: implications from a lawsonite eclogite from the Dominican Republic. European Journal of Mineralogy 16, 909-916. https://doi.org/10.1127/0935-1221/2004/0016-0909.
- Zack, T. A. (2013). Cold slab-mantle interface: constraints from exceptionally well preserved lawsonite eclogites. Mineralogical Magazine 77, 2574.